

Metadata of the chapter that will be visualized in SpringerLink

Book Title	Marine Renewable Energy	
Series Title		
Chapter Title	Mapping the Ocean Current Strength and Persistence in the Agulhas to Inform Marine Energy Development	
Copyright Year	2017	
Copyright HolderName	Springer International Publishing AG	
Corresponding Author	Family Name	Meyer
	Particle	
	Given Name	I.
	Prefix	
	Suffix	
	Division	Centre for Renewable and Sustainable Energy Studies
	Organization	Stellenbosch University
	Address	Stellenbosch, South Africa
	Email	imke.meyer90@gmail.com imke.meyer90@sun.ac.za
Author	Family Name	Braby
	Particle	
	Given Name	L.
	Prefix	
	Suffix	
	Division	Department of Oceanography
	Organization	University of Cape Town
	Address	Cape Town, South Africa
	Email	laurabraby@gmail.com
Author	Family Name	Krug
	Particle	
	Given Name	M.
	Prefix	
	Suffix	
	Division	Council for Scientific and Industrial Research Natural Resources and the Environment, Earth Observation
	Organization	Nansen-Tutu Centre for Marine Environmental Research, University of Cape Town
	Address	Cape Town, South Africa
	Division	Department of Oceanography
	Organization	University of Cape Town
	Address	Cape Town, South Africa
	Email	mkrug@csir.co.za
Author	Family Name	Backeberg
	Particle	

Given Name	B.
Prefix	
Suffix	
Division	Council for Scientific and Industrial Research, Natural Resources and the Environment, Coastal Systems Group
Organization	Nansen-Tutu Centre for Marine Environmental Research, University of Cape Town; Nansen Environmental and Remote Sensing Center
Address	Cape Town, South Africa
Division	Department of Oceanography
Organization	University of Cape Town
Address	Cape Town, South Africa
Email	bbackeberg@csir.co.za

Abstract	<p>The potential for energy extraction from the fast-flowing Agulhas Current along South Africa's East Coast is examined. Potentially suitable regions are evaluated using state-of-the-art satellite remote-sensing, predictive modelling, and in situ observation technologies. A mid-shelf location (91 m depth) and an offshore location (255 m depth) at approximately 32.51°S and 28.83°E are evaluated using these tools, and it is found that the current core borders on the mid-shelf location and passes over the offshore location with mean velocities of 1.34 m/s and 1.59 m/s, respectively, at the 30 m depth. Current velocity data derived from satellite remote-sensing and predictive models were compared to in situ current measurements from Acoustic Doppler Current Profilers to determine their ability to accurately capture current velocities for future use in the evaluation of energy extraction sites. Although the modelled data's representation of the Agulhas Current's velocities was a better comparison than the satellite product, the predictive model was less representative of the variability in the Agulhas Current. Further examination of the data showed that both the satellite and the predictive model are only able to accurately capture variability in the Agulhas Current on time scales longer than monthly. Despite this, the data provide useful insight into the unique challenges encountered when exploiting the Agulhas Current as a resource for energy generation; in particular, the irregular occurrence of large Agulhas Current meanders (known as Natal Pulses). The proposed energetic region is well positioned with respect to environmental, economic, and social aspects because the nearest medium voltage substation is 30 km from the point of contact at the coastline. The sites are not located within any existing or proposed marine protected areas or prime fishing grounds. If the mooring challenges in water depths of 250 m or greater are overcome, then such a turbine array can make a significant contribution to the South African electricity grid.</p>
----------	---------------------------------------------------------------------------------------------------------------------------------------------------------------------------------------------------------------------------------------------------------------------------------------------------------------------------------------------------------------------------------------------------------------------------------------------------------------------------------------------------------------------------------------------------------------------------------------------------------------------------------------------------------------------------------------------------------------------------------------------------------------------------------------------------------------------------------------------------------------------------------------------------------------------------------------------------------------------------------------------------------------------------------------------------------------------------------------------------------------------------------------------------------------------------------------------------------------------------------------------------------------------------------------------------------------------------------------------------------------------------------------------------------------------------------------------------------------------------------------------------------------------------------------------------------------------------------------------------------------------------------------------------------------------------------------------------------------------------------------------------------------------------------------------------------------------------------------------------------------------------------------------------------------------------------------------------------------------------------------------------------------------------------------------------------------------------------------------------------------------------------------------------------

Keywords (separated by '-')	Agulhas current - Marine energy - Ocean modelling - Satellite remote sensing - Acoustic Doppler Current Profiler - Natal pulses
--------------------------------	---------------------------------------------------------------------------------------------------------------------------------



Mapping the Ocean Current Strength and Persistence in the Agulhas to Inform Marine Energy Development

I. Meyer, L. Braby, M. Krug and B. Backeberg

Introduction

Renewable energy technology has undergone tremendous development over the last three decades and has found great commercial success in the onshore and offshore wind, solar, and biomass spheres. Of the renewable energy technologies, ocean energy technology is the least developed, and due to the vastness of the resource, many facets are yet to be fully understood. Energy in the world's oceans is found in either kinetic (i.e. waves, tides, or currents) or potential (i.e. thermal or salinity gradients) forms, and all forms are being investigated to generate useful electric power.

The focus of this study is ocean current energy, the kinetic energy available in large-scale open-ocean geostrophic surface currents, and specifically the Agulhas

I. Meyer (✉)

Centre for Renewable and Sustainable Energy Studies,
Stellenbosch University, Stellenbosch, South Africa
e-mail: imke.meyer90@gmail.com; imke.meyer90@sun.ac.za

M. Krug

Council for Scientific and Industrial Research Natural Resources and the Environment,
Earth Observation, Nansen-Tutu Centre for Marine Environmental Research,
University of Cape Town, Cape Town, South Africa
e-mail: mkrug@csir.co.za

B. Backeberg

Council for Scientific and Industrial Research, Natural Resources and the Environment,
Coastal Systems Group, Nansen-Tutu Centre for Marine Environmental Research,
University of Cape Town; Nansen Environmental and Remote Sensing Center,
Cape Town, South Africa
e-mail: bbackeberg@csir.co.za

L. Braby · M. Krug · B. Backeberg

Department of Oceanography, University of Cape Town, Cape Town, South Africa
e-mail: laurabraby@gmail.com

16 Current. Western boundary ocean currents have become an area of focus (Duerr and
17 Dhanak 2012; Chang et al. 2015), and the Agulhas Current is of specific interest in
18 the Southern Hemisphere (Meyer et al. 2014; VanZwieten et al. 2014, 2015). Each
19 ocean current has its own features but most western boundary currents have similar
20 characteristics. Western boundary currents are narrow, intense, flow poleward, and
21 are driven by the zonally integrated wind stress curl of the adjacent basins (Lut-
22 jeharms 2006).

23 Western boundary currents generally exhibit their strongest flow near the
24 ocean's surface. In recent years, interest in these currents has evolved closer to
25 commercial development, so the physical characteristics of the currents and their
26 possible impacts on power generation need to be identified and fully understood.
27 Ocean current resource characterisation studies have been performed for the Gulf
28 Stream in the United States (Duerr and Dhanak 2012; Haas et al. 2013) and the
29 Kuroshio Current near Japan and Taiwan (Chen 2010). Studies of the Agulhas
30 Current on the East Coast of South Africa (e.g. Lutjeharms 2006; Beal and Bryden
31 1999; Bryden et al. 2005) have focused predominantly on understanding
32 open-ocean oceanographic and climate-related processes. Few studies focus on
33 characterising the Agulhas Current for ocean energy extraction technologies; in
34 particular, the ocean current dynamics near the continental shelf region where
35 technology deployment is possible are poorly understood.

36 Western boundary currents have the potential to be more reliable sources of
37 energy than erratic winds because of their inherent reliability, persistence, and
38 strength. Further, water is approximately 1,000 times denser than air resulting in
39 high energy density in the oceans. Recent investigations by Haas et al. (2013) have
40 shown that the Gulf Stream could potentially have an average power dissipation of
41 18.6 GW or 163 TWh/yr (serving the electricity needs of approximately 16 million
42 households). According to the Ocean Energy Council, "Ocean currents are one of
43 the largest untapped renewable energy resource on the planet. Preliminary surveys
44 show a global potential of over 450,000 MW, representing a market of more than
45 US\$550 billion" (Renewable Energy Caribbean 2014).

46 The Agulhas Current flows southward along South Africa's East Coast, as a fast
47 and narrow stream, and transports on average 80 million cubic metres of water per
48 second (Beal et al. 2015). Studies of the northern extent (north of 35°S) of the
49 current have shown that its course closely follows the narrow continental shelf
50 (Gründlingh 1983), meandering less than 15 km from its mean path, and that the
51 core of the current lies within 31 km from the coast almost 80% of the time (Bryden
52 et al. 2005). The intensity of the current, its close proximity to the coast, and its
53 relative stability make the Agulhas Current one of the more attractive ocean cur-
54 rents in the world to exploit for energy extraction.

55 However, the stable trajectory of the current is intermittently interrupted by
56 perturbations known as Natal Pulses—large solitary meanders that form at the Natal
57 Bight, a region between 29 and 30°S, and propagate downstream in the Agulhas
58 Current at ± 10 km/day (Lutjeharms and Roberts 1988). Fluctuations in the Agul-
59 has Current path associated with these meanders do not display the same frequency
60 characteristics at all latitudes (Rouault and Penven 2011), because of the dissipation

61 mechanisms of the Natal Pulses as they propagate downstream. Variability in the
62 current and its velocities occurs across of a range of temporal and spatial scales
63 (Lutjeharms 2006), and understanding, monitoring, and predicting these are vital
64 for the effective use of the Agulhas Current as a renewable energy resource.

65 One of the most effective ways to monitor ocean currents over large spatial areas
66 at a relatively high temporal frequency is through the use of satellite measurements.
67 While ocean currents cannot be directly measured from space at present (Dohan and
68 Maximenko 2010), surface current information can be derived from a range of
69 remotely sensed observations to study and monitor the ocean circulation. At the
70 larger scales (tens of kilometres), geostrophic currents, which occur as a result of
71 pressure and Coriolis forcing, often drive most of the circulation. Wind stress at the
72 ocean's surface also drives transport that can be estimated using the Ekman theory
73 (Ekman 1905). Satellite observations of ocean surface winds and sea surface height
74 (SSH) have therefore widely been used over the last two decades to study and
75 monitor ocean circulation (Robinson 2004). Other remote-sensing observations
76 such as Sea Surface Temperature (SST) and sea surface roughness can also be used
77 routinely and systematically to derive ocean current information. The Agulhas
78 Current is associated with strong signatures in SSH, SST, and sea surface rough-
79 ness, all of which have been exploited successfully to study the variability of the
80 Agulhas Current as demonstrated by Rouault et al. (2010), Rouault and Penven
81 (2011), and Krug and Tournadre (2012). When used in synergy with the global
82 network of in situ surface drifters, satellites can provide improved global obser-
83 vations of the sea surface velocity.

84 However, satellite measurements are limited to the surface and for the purpose of
85 marine energy extraction, it is important to have information about the vertical
86 structure of the water column. Measurements of the vertical structure of the ocean
87 are even sparser. To deal with the spatially and temporally incoherent observations
88 of the oceans, we use numerical models combined with observations through a
89 process called data assimilation. Realistic simulations of the Agulhas system are
90 complicated by the highly nonlinear nature of the mesoscale variability governing
91 the Agulhas Current (Bia stochastic et al. 2008). Even if a model is capable of repre-
92 senting the mean circulation and variability of the region, inaccuracies in the initial
93 state estimate inhibit the forecast skill of the model up to the decadal time scale
94 (Meehl et al. 2009). Data assimilation provides the means to estimate a physically
95 consistent three-dimensional (3D) estimate of the ocean state, combining a
96 dynamical forecast model and observations together with their relative errors. Due
97 to inaccurate numerics and boundary conditions, model solutions are imperfect. By
98 repeatedly assimilating data, models may be constrained to provide a more realistic
99 estimate of the ocean state. Such data-assimilative models of the ocean play a vital
100 role in predicting ocean currents as well as in understanding the 3D structure and its
101 variability.

102 By combining state-of-the-art satellite remote-sensing observations with
103 data-assimilative (predictive) ocean models, this study aims to identify areas of
104 energetic flow along South Africa's East Coast for the purpose of marine energy
105 extraction and to examine the associated current characteristics. The ability and

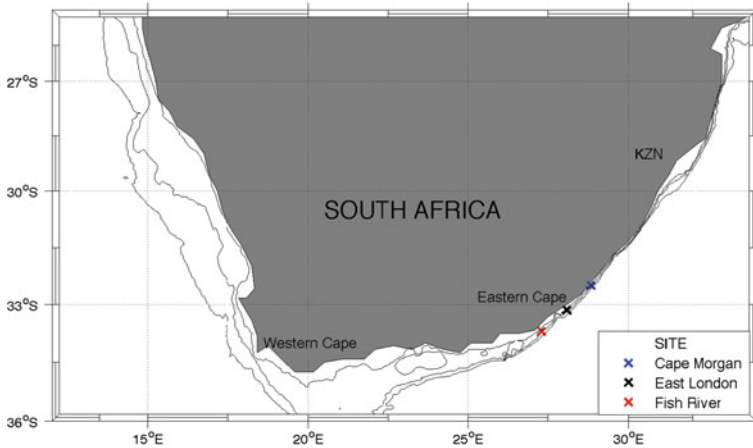


Fig. 1 Position of ADCP deployments with 100, 200, and 500 m isobaths

106 usefulness of the satellite remote-sensing observations and predictive models to
 107 monitor and predict current velocities and their variability will be assessed by
 108 comparing them with in situ velocity measurements from Acoustic Doppler Current
 109 Profilers (ADCPs) for the period from 2009 to 2010. In doing so, the impact of the
 110 current behaviour on the potential power production will be quantified, and the
 111 present day state-of-the-art tools used to accurately monitor and predict fluctuations
 112 in the Agulhas Current that affect power production will be critically examined.

113 The focus area for the analysis lies between the latitudes of 31 and 34°S as
 114 indicated in Fig. 1. The coastal proximity and strength of the Agulhas Current in
 115 the southeast Agulhas Current region make it the most suitable region for energy
 116 exploitation. Farther south, the Agulhas Current flows too far from the coast to
 117 allow for efficient energy recovery. Farther north, the current strength is decreased.

118 This chapter examines the Agulhas Current characteristics and attempts to
 119 quantify how its behaviour will affect potential power production. In the following
 120 section, the available data and data types are described, followed by an investi-
 121 gation of current strength and variability, the usefulness of the various data sets, and
 122 the implications for possible energy production. The technical, environmental, and
 123 social impacts of harnessing energy from the Agulhas Current are also considered.

124 Data and Methods

125 The data sets described in the following sections are used to determine the physical
 126 characteristics of the Agulhas Current. The sections also address the relative use-
 127 fulness of each data set towards reducing the barriers of entry into the ocean current
 128 energy market.

GlobCurrent Data Set

In this study, we use the combined 15-m-depth GlobCurrent Version 2 product, which is available from the GlobCurrent project (<http://www.globcurrent.org/>). This data set consists of 13 years of global gridded ocean current fields and is provided at a 0.12° spatial resolution and 3-hour time interval. The combined current in the GlobCurrent data set is computed as the sum of the geostrophic and Ekman components of the flow. In the GlobCurrent product, geostrophic currents are derived from satellite observations of SSH from multiple altimeters, while the Ekman currents (driven by local wind forcing) are estimated using Lagrangian ocean current information collected from surface drifters and Argo floats. A detailed description of the method used to derive the GlobCurrent geostrophic and Ekman ocean currents is provided by Rio et al. (2014).

Confirming the validity of using satellite data to monitor the behaviour of the Agulhas Current is crucial to reducing the costs of monitoring the operations of a potential ocean current plant as well as monitoring upstream events that can affect the potential power output of a plant.

Global Hybrid Coordinate Ocean Model

3D ocean forecast data from a global Hybrid Coordinate Ocean Model (HYCOM) are used in this study. These data are freely available from the HYCOM consortium (hycom.org), a multi-institutional effort sponsored by the National Ocean Partnership Program, as part of the U.S. Global Ocean Data Assimilation Experiment, to develop and evaluate a data-assimilative hybrid isopycnal-sigma-pressure (generalised) coordinate ocean model.

The numerical model is configured for the global ocean, and computations are carried out on a Mercator grid between 78°S and 47°N at $1/12^\circ$ (± 7 km) resolution. There are 32 vertical layers, and the model's bathymetry is derived from a quality-controlled Naval Research Laboratory Digital Bathymetry Data Base 2-minute resolution data set. Surface forcing data are from the Navy Operational Global Atmospheric Prediction System and include wind stress, wind speed, heat flux (using bulk formula), and precipitation.

The data assimilation scheme used is the Navy Coupled Ocean Data Assimilation system (Cummins 2005), which uses the model forecast as a first guess in a Multi-Variate Optimal Interpolation scheme and assimilates available along-track satellite altimeter observations (obtained via the NAVOCEANO Altimeter Data Fusion Center), satellite and in situ SST as well as available in situ vertical temperature and salinity profiles from Expendable BathyThermographs, ARGO floats, and moored buoys. The surface measurements are projected to the model interior using the Modular Ocean Data Assimilation System (Fox et al. 2002).

On a daily basis, 5-day hindcasts and 5-day forecasts are produced. The raw data are interpolated to 33 fixed horizontal levels, which are 0, 10, 20, 30, 50, 75, 100, 125, 150, 200, 250, 300, 400, 500, 600, 700, 800, 900, 1,000, 1,100, 1,200, 1,300, 1,400, 1,500, 1,750, 2,000, 2,500, 3,000, 3,500, 4,000, 4,500, 5,000, and 5,500 m.

U- and v-component velocities from 1 December, 2009 to 31 January, 2013 were downloaded and subset to 25–35°E and 27–36°S. The data were generated by two experiments. The first experiment (expt_90.8) ended on 2 January, 2011, after which expt_90.9 was used. The two experiments are subtly different in that the top layer in expt_90.9 was 1 m thick (as opposed to 3 m in expt_90.8). This difference is not expected to affect our analysis.

The ability to predict the behaviour of the Agulhas Current will be advantageous for the integration of any future power plants into the national power pool. Accurate forecasts at a high temporal resolution will ensure the maximum utilisation of an ocean current power plant.

Acoustic Doppler Current Profilers

Between 2005 and 2010, the South African electricity utility, Eskom, conducted a series of in situ current measurements along the eastern shores of South Africa as part of a preliminary assessment of the Agulhas Current as a source of energy. The in situ ocean currents were measured using moored ADCPs at selected sites along the continental shelf and in water depths ranging from 96 to 60 m. All ADCPs sampled ocean current velocities throughout the water column in 2-m-high vertical bins. Bins from different deployments were concatenated by linking together measurements from the closest bin (nearest bin approach). A summary of this ADCP data is provided in Table 1.

It is observed that the ADCP measurements (Table 1) were taken at the periphery of the current. Rouault and Penven (2011) have found that the core of the current is located between 20 and 50 km from the shore and approximately above the 200 m isobath. Note that the dates on which each data set was recorded do not coincide and this can possibly lead to a bias towards one site.

Between 2012 and mid-2013, an additional two ADCPs were deployed at a mid-shelf and offshore location and resulted in an 18-month period of continuous data in the region of 28.8°E and 32.5°S. The details of the captured data are outlined in Table 2. The data were collected using Teledyne RDI ADCPs with a 60-min temporal resolution. Viable data for the mid-shelf location range from 84 to 10 m below the sea surface and for the offshore location, and from 238 to 22 m below the sea surface.

Table 1 Details of in situ ADCP measurements

ADCP site name	Instrument type	Longitude (E)	Latitude (S)	Water depth (m)	Record length	Sampling interval (h)
Cape Morgan CM305	RDI 300	28.83183	32.50733	89	2009/12/05-2010/03/03	1
Cape Morgan CM306	RDI 300	28.83179	32.50725	87	2010/03/03-2010/09/13	1
Fish River FR308	RDI 300	27.29750	33.70335	88	2009/12/04-2010/03/04	1
Fish River FR309	RDI 300	27.29745	33.71332	91	2010/03/04-2010/09/03	1
East London EL314	RDI 300	28.00866	32.15145	82	2009/12/04-2010/03/03	1
East London EL315	RDI 300	28.08651	33.15140	85	2010/03/03-2010/09/13	1

Table 2 Deployment series 2: details of available ADCP data

Location	ADCP type/bin resolution (m)	Distance from shore (km)	Time period	Sounding depth (m)
Mid-shelf	RDI 300/2	14	2012/01/24-2013/06/30	91
Offshore (edge of shelf)	RDI 150/6	18	2012/01/24-2013/06/30	255

Current Strength and Variability

Comparison GlobCurrent, HYCOM, ADCPs

To compare the three ocean velocity products, Principal Component Analysis (PCA) was applied to the ADCP velocity data as well as the GlobCurrent and HYCOM data at the same locations (Cape Morgan, East London, and Fish River) and depths. PCA decomposes data in terms of orthogonal basis functions to find time series and spatial patterns (Wold et al. 1987). The two eigenvectors contain most of the details about the data. They were computed and plotted as 95% confidence interval ellipses in Fig. 2 and represent the two dominant directional modes of the measured current velocities at the three selected locations, indicating the dominant current direction as well as its lateral variation.

Figure 2 provides a good overview of the Agulhas Current time-averaged strength as well as its overall variability. Comparisons between the in situ satellite and numerical model output data sets show distinct differences. From the in situ

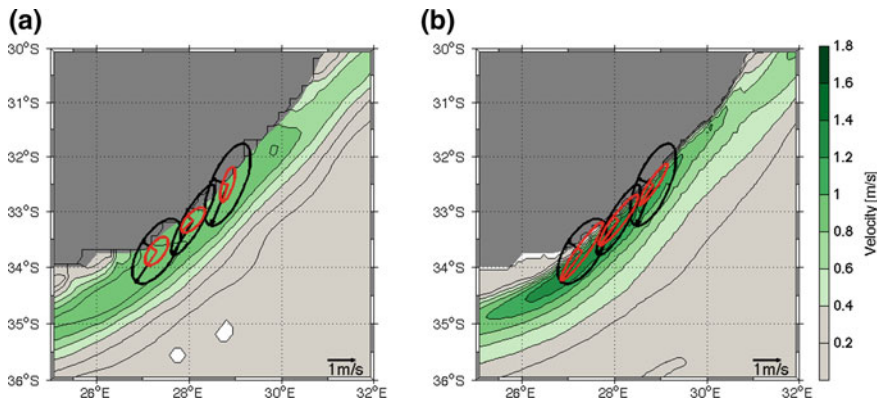


Fig. 2 **a** Map of Agulhas time-averaged currents from the GlobCurrent product with overlaid current ellipses from ADCP data (*black*, at 20 m or in the upper layer best suited for energy production) and GlobCurrent data (*red*, at 15 m depth), and **b** map of Agulhas time-averaged currents from the HYCOM product with overlaid current ellipses from ADCP data (*black*, at 20 m or in the upper layer best suited for energy production) and HYCOM data (*red*, at same depth as ADCPs)

ADCP data, it is seen that the Cape Morgan location is the most energetic and has the strongest major velocity component. This finding is reiterated by the GlobCurrent data but not by the HYCOM data.

Comparing the ADCP and GlobCurrent ellipses (Fig. 2a, black and red, respectively), it is evident that although the direction of flow is similar, there are significant differences between the two data sets at all three locations. The ADCP data indicate a much stronger south-westward flowing velocity component with larger lateral variations compared to the GlobCurrent data.

The HYCOM velocity map (Fig. 2b) indicates that the data-assimilative modelling system is able to produce high mean velocities, and comparing the HYCOM ellipses to the ADCP ellipses suggests that the mean south-westward component is better represented than in GlobCurrent, but the lateral variability seems to be reduced in HYCOM.

In agreement with the current ellipses (Fig. 2a), the major and minor velocity components summarised in Table 3 confirm that the GlobCurrent data underestimate the ADCP measured current velocity by $\pm 60\%$. While there is a slight improvement in HYCOM, the data-assimilative modelling system still underestimates the measured ADCP velocities (Table 4). It is important to note the differences between satellites remotely sensed, modelled, and in situ observed data because these differences could lead to incorrect site selection and evaluations for energy production. Further, if the HYCOM data set is used as a first step towards identifying energetic regions prior to deploying in situ measurement devices, this data set would lead to incorrect assumptions about the most energetic region. Further, the significant under prediction seen in the GlobCurrent data set can result in termination of further exploration.

Table 3 Details of the time-averaged velocity vector lengths of the GlobCurrent and ADCP measurements

Site name	ADCP data		GlobCurrent	
	Major component (m/s)	Minor component (m/s)	Major component (m/s)	Minor component (m/s)
CM	1.6710	0.6850	0.6815	0.2377
EL	1.5496	0.3959	0.6475	0.2769
FR	1.4216	0.6997	0.6564	0.3251

Table 4 Details of the time-averaged velocity vector lengths of the HYCOM and ADCP measurements

Site name	ADCP data		HYCOM	
	Major component (m/s)	Minor component (m/s)	Major component (m/s)	Minor component (m/s)
CM	1.6710	0.6850	0.9794	0.1918
EL	1.5496	0.3959	1.2333	0.2542
FR	1.4216	0.6997	1.3730	0.2443

242 The observed underestimation of both GlobCurrent and HYCOM may have to
 243 do with the temporal averaging of the data in their generation. The regularly gridded
 244 satellite data (GlobCurrent) are produced using optimal interpolation and merging
 245 techniques to fill the gaps between spatially sparse satellite ground tracks. This
 246 merging process results in the smoothing of the data in both space and time (Ducet
 247 et al. 2000) and the underestimation of the ocean current velocities. The underes-
 248 timation observed in HYCOM may be associated with the combined effect of the
 249 model itself underestimating the currents in addition to the assimilation of satellite
 250 products into the model.

251 The impact of spatial and temporal smoothing is examined below, by performing
 252 a spectral analysis (Fig. 3), whereby the dominant frequencies of variability in the
 253 three data sets are compared. Then, temporal smoothing (daily, weekly, 10-daily,
 254 and monthly) is applied to the ADCP data and plotted in a Taylor Diagram (Fig. 4),
 255 which is a way to graphically summarise how closely a set of data matches a
 256 reference data set (in this case the hourly ADCP data).

257 A spectral analysis essentially transforms magnitude—time data into variance—
 258 frequency space. Figure 3 shows the spectra from the ADCP data (a), GlobCurrent
 259 data (b), and HYCOM data (c) for the Cape Morgan and East London locations.

260 Variability in the Agulhas Current can occur at a number of time scales, which is
 261 evident from examining the ADCP data. Some examples of variability include
 262 tides, sub-mesoscale and mesoscale eddies, Natal Pulses, seasonal variations in
 263 current velocities (Krug and Tournadre 2012), and longer term variations associated
 264 with climate modes such as the El Niño Southern Oscillation and gyre circulation
 265 changes. The ADCP spectra were compared with the GlobCurrent and HYCOM

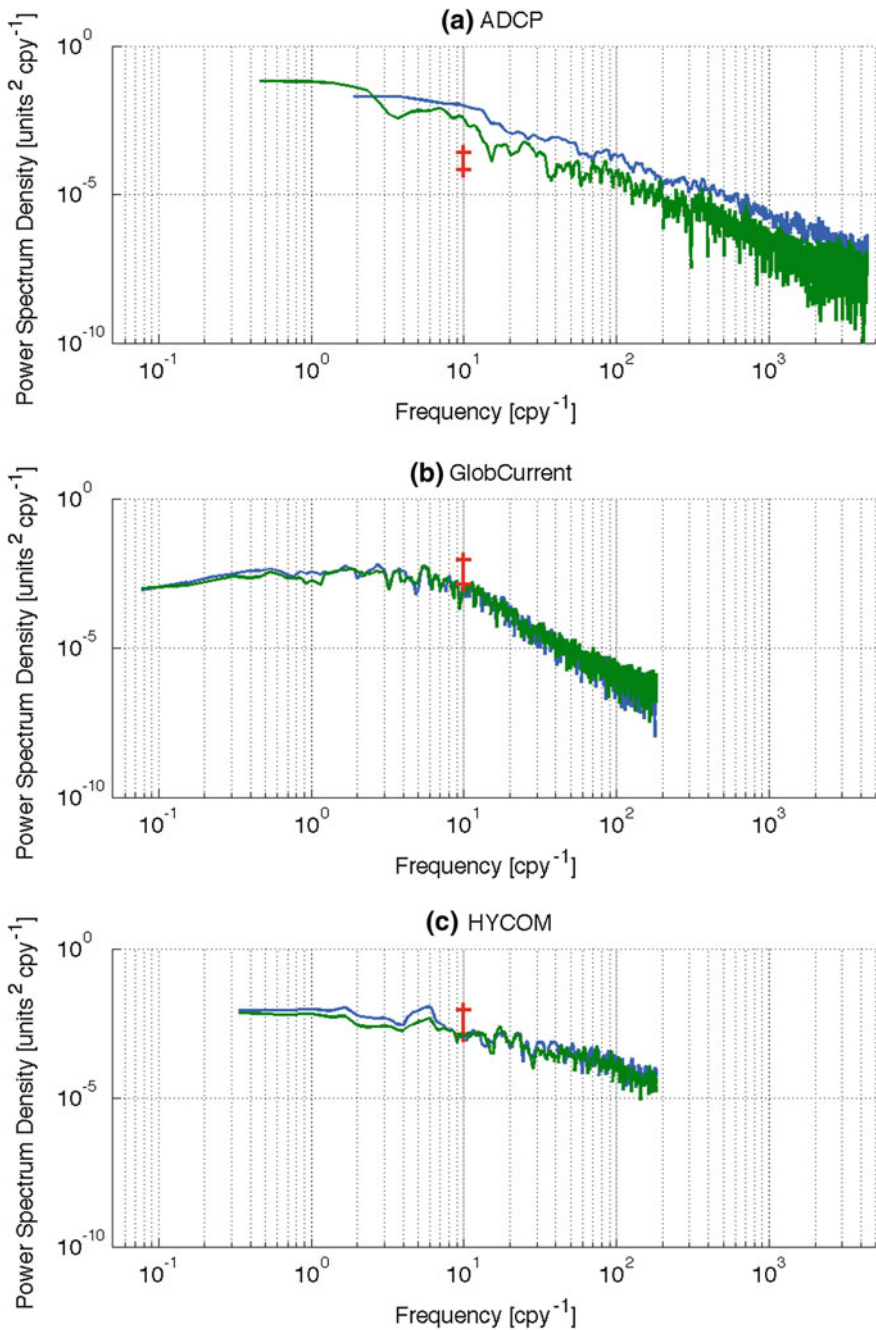


Fig. 3 Spectra at selected sites—Cape Morgan (green) and East London (blue)—using **a** ADCP data for record data lengths of 193 days (green) and 137 days (blue), **b** GlobCurrent data for a record data length of 14 years, and **c** HYCOM data for a record data length of 3 years. The red line indicates the 95% significance level

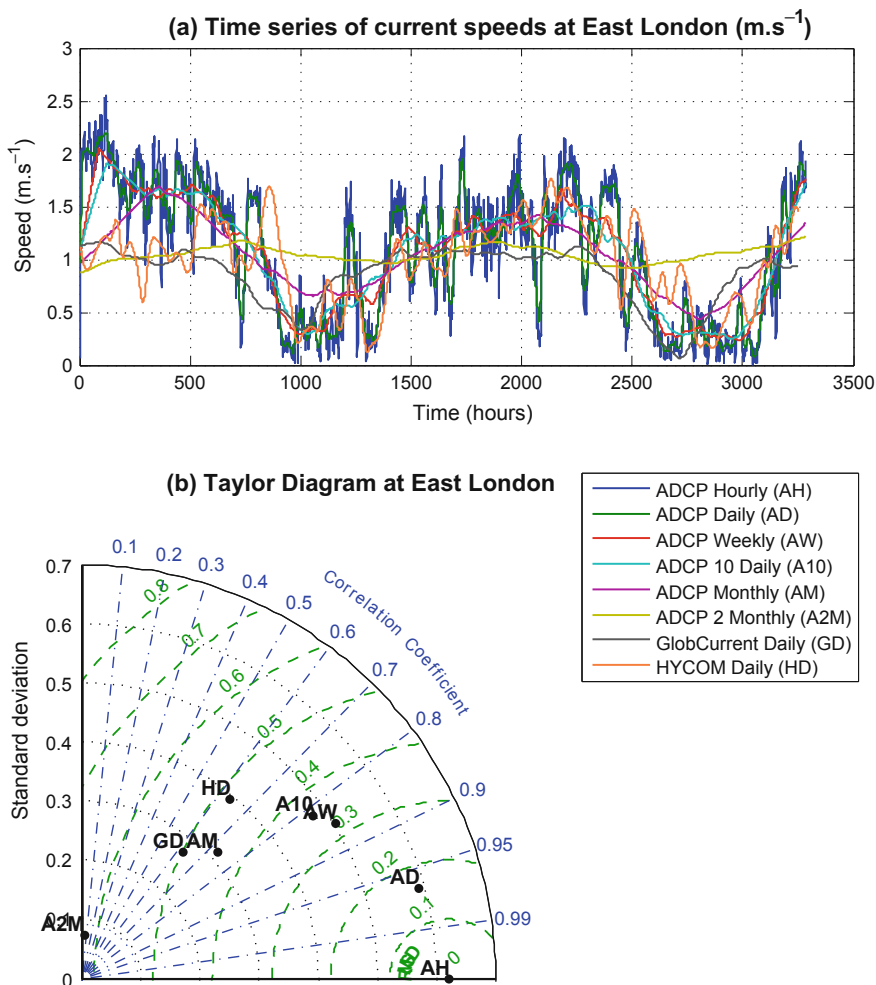


Fig. 4 **a** A time series of Agulhas Current speeds (m/s) at East London using hourly, daily, weekly, 10-daily, monthly, and 2-monthly ADCP data as well as daily GlobCurrent and HYCOM data at the same location. **b** A Taylor Diagram showing the standard deviation, correlation, and centred root-mean-square difference of the same data sets at East London

266 spectra to evaluate the accuracy of the modelled and satellite-derived velocities with
 267 respect to these modes of variability.

268 Comparing the three data sets, it is evident that there is very little difference
 269 between the Cape Morgan and East London spectra in the GlobCurrent and
 270 HYCOM data sets. The ADCP data set, however, shows a higher spectrum density
 271 at the East London location. This suggests that there are slightly higher levels of
 272 variability at East London compared to Cape Morgan, which is in agreement with
 273 the PCA analysis (Fig. 2).

To determine the frequency of the dominant mode of variability, one evaluates where the strongest change in the slope of the spectra occurs. The x-axis of Fig. 3 represents frequency, where 100 is 1 cycle per year. Each successive vertical grid line to the right is one additional cycle per year. Thus, the GlobCurrent data indicate a predominant mode of variability of six cycles per year (two-monthly), which may be related to the passage of Natal Pulses or other Agulhas Current meanders. This two-monthly cycle is also present in HYCOM, but the change in slope is much weaker, and therefore, the signal is not significant. The lengths of the ADCP time series (193 days at Cape Morgan, 137 days at East London,) are too short to confidently confirm the two-monthly dominant mode of variability.

Typically, spectra of ocean processes should have steep slopes, which signify an inverse cascade of energy from low frequencies to high frequencies (e.g. hourly to monthly) (Scott and Wang 2005). The slopes in the spectra of the ADCP and GlobCurrent data sets are in good agreement with each other, indicating a rapid decay in the ocean current energy towards high frequency. At higher frequencies (101–102), the HYCOM data set has more energy compared to the ADCP and GlobCurrent data sets, but the slope is flatter indicating that all frequencies have similar levels of energy, which is indicative of white noise. The flatter slope in the HYCOM data set shows that energy decay in the model is inadequately simulated and that in the assimilated model output, there are no coherent processes producing an inverse energy cascade. The fact that the slopes of the inverse energy cascade in the spectra of GlobCurrent and the ADCP data agree indicates that both data sets are able to capture the larger (meso) scale processes that dominate the energy spectra. Comparatively, the higher frequency variability is relatively less important, as is evident in the flattening of the slope.

Figure 4a shows the time series of the hourly ADCP data, the daily, weekly, 10-daily, monthly, and 2-monthly averaged ADCP data, as well as the GlobCurrent and HYCOM daily data for East London. The comparison highlights the impact of temporally averaged data as well as the variability captured by the temporally smoothed ADCP data and the daily satellite and modelled data products. The correlation coefficient, standard deviation, and root-mean-square difference (RMSD) of the temporally averaged ADCP data together with the GlobCurrent and HYCOM data are summarised in the Taylor Diagram (Fig. 4b).

As expected, the correlation coefficient and standard deviation decrease, concurrently with increasing RMSD when the ADCP is averaged over increasingly longer time periods (i.e. hourly to daily to weekly to monthly to two-monthly).

Using the hourly ADCP data as a reference, and comparing the respective daily, weekly, 10-daily, monthly, and 2-monthly averaged ADCP data to the daily GlobCurrent and HYCOM data, suggests that HYCOM and GlobCurrent are only able to accurately represent variability occurring at the monthly time scale. This is indicated by the fact that the monthly ADCP data and the GlobCurrent and HYCOM daily data are clustered around similar correlation coefficients, standard deviations, and RMSDs.

These results have significant implications for the ability to use state-of-the-art satellite remotely sensed and assimilative modelling products when determining

319 potential energy extraction sites. Furthermore, the ability to use these tools to
320 predict variability in the Agulhas Current is questionable at this stage, and this
321 highlights the need for further development and improvement of these products.
322 Nevertheless, in the absence of a spatial and temporally coherent ocean observing
323 system for the Agulhas Current, these data provide useful insights into the modes of
324 variability of the Agulhas Current and their implications for energy production.

325 *Implications for Energy Production*

326 For resource measurements to be useful in monitoring or predicting behaviour, the
327 temporal resolution of the data used in the prediction need to be able to capture the
328 temporal variability associated with the ocean processes to be predicted. For
329 example, if significant variability is seen at an hourly resolution, then the moni-
330 toring equipment needs to be able to accurately capture this variability to be able to
331 successfully control a potential ocean current power plant. As noted in the above
332 analysis, in situ ADCP data are the only data at present that can accurately capture
333 the full variability of the Agulhas Current, but deploying and managing ADCP
334 devices are costly and spatially limiting. In the absence of ADCP data, the only
335 alternative data sources are those derived from satellite remote-sensing measure-
336 ments and data-assimilative predictive models. In the previous section, it is shown
337 that the correlation between data obtained from the ADCPs and those obtained from
338 the Globcurrent and HYCOM products only compare well on a monthly scale and
339 thus have limited use in assisting in monitoring and predicting the shorter time
340 scales of variability in the Agulhas Current. Additionally, satellite remote-sensing
341 observations are limited to the surface level, so it is important to note that there is a
342 need for the characteristics throughout the depth of the water column to characterise
343 to be useful in monitoring and predicating energy output from this resource.

344 Figure 5 shows time series ADCP data plots of velocity versus depth high-
345 lighting the variability of the Agulhas Current. The presence of major events of
346 variability—a Natal Pulse—is recognised as a drop in the current speed to near zero
347 throughout the water column for longer than 10 continuous days. This indicates that
348 the current core has been displaced seaward from its original course by the Natal
349 Pulse meander. All measurements taken at different latitudes have been plotted on
350 the same temporal axis so that the propagation of a Natal Pulse southward along the
351 coastline can be identified.

352 In Fig. 5a, the presence of four Natal Pulses, which occurred in Nov 09, Mar 10,
353 May 10, and Aug 10 and each persisted for at least 20 days, is seen from November
354 2009 to September 2010. In Fig. 5c, it is seen that the Natal Pulses of November
355 2009–September 2010 in Fig. 5b did not dissipate as they travelled southward, and
356 the presence of these pulses is seen in the data set in Fig. 5c.

357 Each of these pulses takes approximately 15–20 days to travel down the coast
358 between the two locations. Similarly, the Natal Pulse that occurred in July 2008
359 travelled down the coast; the Pulse is first seen in the data set captured in Fig. 5a,

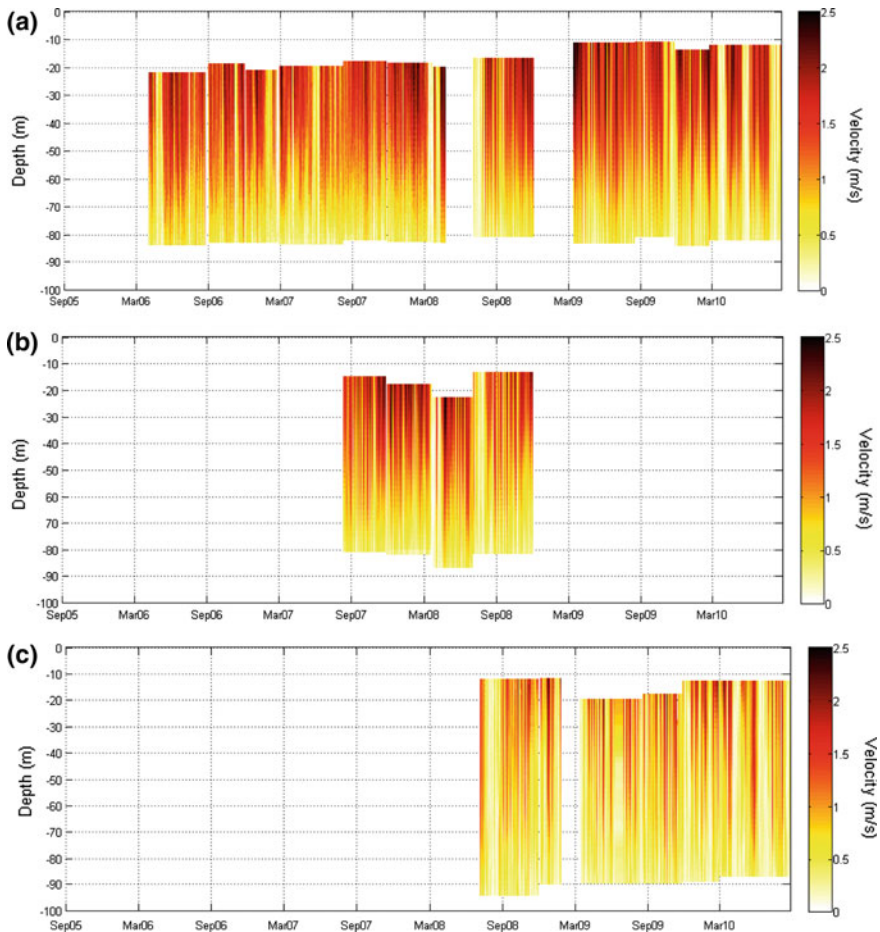


Fig. 5 Temporal plots of velocity magnitude versus depth at **a** Cape Morgan, **b** East London, and **c** Fish River

360 then again in the Fig. 5b data set, and lastly in the Fig. 5c data set. This Natal Pulse
 361 also takes approximately 15 days to arrive at the location plotted in Fig. 5c from the
 362 location plotted in Fig. 5a. The fact that the Natal Pulse took a fortnight to travel
 363 ~200 km is a testament to the sluggish velocity magnitude at which such pulses
 364 propagate.

365 Figure 5a, shows the results from two deployed ADCPs, one deployed from
 366 April 2006 to May 2008 and another from March 2009 to September 2010. When
 367 the two time periods are compared, the 24-month period from April 2006 to May
 368 2008 only sees three pulses of approximately 10-days duration whereas during the
 369 17-month period from March 2009 to September 2010 four Natal Pulses are
 370 observed. The difference in the occurrence of Natal Pulses at the same location over

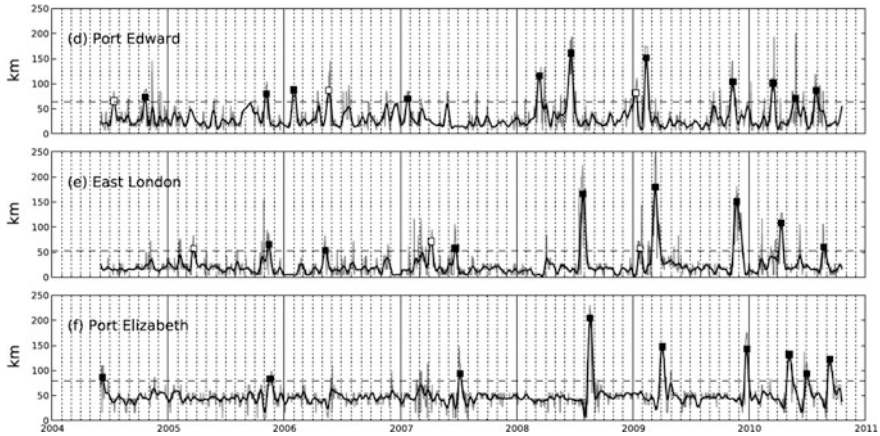


Fig. 6 Position of the Agulhas Current used to identify the presence of Natal Pulses. Natal Pulses are indicated by black squares, adapted from Fig. 5 in Rouault and Penven (2011)

371 different time periods shows the erratic and unpredictable nature of this phe-
372 nomenon and emphasises the importance of anticipating such events.

373 The results found in the temporal velocity magnitude plots compare well with
374 the results found by Rouault and Penven (2011). Figure 6 shows the position of the
375 Agulhas Current inshore front relative to the shore at three locations along the
376 coastline in order to determine the presence and propagation of Natal Pulses. It is
377 promising to see the correlation between the in situ data presented in Fig. 5a and the
378 satellite data used to plot Fig. 6e. From Fig. 6, it is seen that the occurrence of the
379 four Natal Pulses from November 2009 to September 2010 is abnormally high;
380 Rouault and Penven (2011) found the average to be 1.6 pulses a year when con-
381 sidering a 20-year period. Further, the same propagation trend down the coastline
382 that was found in Fig. 5 is shown in Fig. 6.

383 The lag between the locations shows the sluggish nature of the phenomenon but
384 can be used to the advantage of plant operators. If an ocean current power plant
385 were to be installed in the energetic region of 32.5°S and the behaviour of the
386 Agulhas Current were tracked further up the coast around 31.2°S , the presence of
387 an approaching Natal Pulse could be predicted approximately two weeks in
388 advance. Such tracking may be done using a remote-sensing technique, but the
389 reduced correlation between in situ and satellite data at the weekly to 10-day
390 time scale (Figs. 5 and 6) may hamper this ability.

391 A timely warning of the occurrence of Natal Pulses is critical, however, and will
392 allow power grid operators to plan to use the period when a Natal Pulse is present
393 for maintenance of the ocean current power plant. Furthermore, grid planners can
394 mobilise other capacity to ensure the demand of the country is met. However, other
395 available capacity may not be available during winter months when demand is high,
396 and because there is no seasonal trend in the occurrence of Natal Pulses, there is
397 risk related to the firm capacity of an ocean current power plant. The lengthy

398 presence of a pulse (~20 days) in one location is a concern for the technically
399 possible capacity factor and the capability of ocean current energy to supply a
400 reasonably uninterrupted supply of power to off-takers..

401 **Characteristics of Energetic Region**

402 From the analysis in current strength and variability section, of the data collected
403 along the South African East Coast, the energetic region lies in the region of 28.8 E
404 and 32.5 S (Cape Morgan location). This location has favourable velocities and
405 because of the bathymetry in the region the current core lies in close proximity to
406 the coast. The following analysis presents the physical characteristics of a mid-shelf
407 and offshore site in this region.

408 ***Current Magnitude***

409 Figure 7 shows the current velocity magnitude versus depth. A minimum, 75%
410 exceedance, 50% exceedance, 15% exceedance, and the current maximum are
411 plotted.

412 When comparing the two sites, the presence of the Agulhas core is seen clearly
413 at the offshore location, where at water depths of 50 and 30 m the mean velocity
414 magnitude is 1.49 and 1.59 m/s, respectively. For the mid-shelf deployment, the
415 mean current velocity magnitude is 1.00 and 1.34 m/s at water depths of at 50 and
416 30 m, respectively. The mid-shelf mooring is thus placed at the core's edge. At the
417 30 m water depth, the offshore current velocity magnitude is 1.2 times greater than
418 the mid-shelf velocity magnitude, which is when the cubed relationship between
419 velocity magnitude and power is considered, results in a significant difference. The
420 75% exceedance values at the 30 m depth are 1.0 and 1.29 m/s for the mid-shelf and
421 offshore deployments, respectively; the 75% exceedance values at the 50 m depth
422 are 0.69 and 1.17 m/s for the respective deployments. A similar trend is seen for the
423 15% exceedance plot; values for the respective mid-shelf and offshore deployments
424 at the 30 m depth are 1.91 and 2.16 m/s and at the 50 m depth they are 1.45 and
425 2.06 m/s. These ranges indicate that a turbine that is deployed in the Agulhas
426 Current will need to operate at speeds between 0.6 and 2 m/s.

427 Figures 8 and 9 are temporal time series plots of time versus depth in which the
428 colour scale indicates the current velocity magnitude for each location. These plots
429 highlight the variability of the current velocity magnitude and show the erratic
430 presence of day-long eddies and Natal Pulses. The distinct presence of a Natal Pulse
431 is seen during April 2013, as indicated by the entire water column velocity mag-
432 nitude dropping to near zero. The size of these meanders are realised because both
433 sites are affected by this occurrence. Figures 8 and 9 show how problematic the
434 presence of this phenomenon will be to potential power production from a turbine

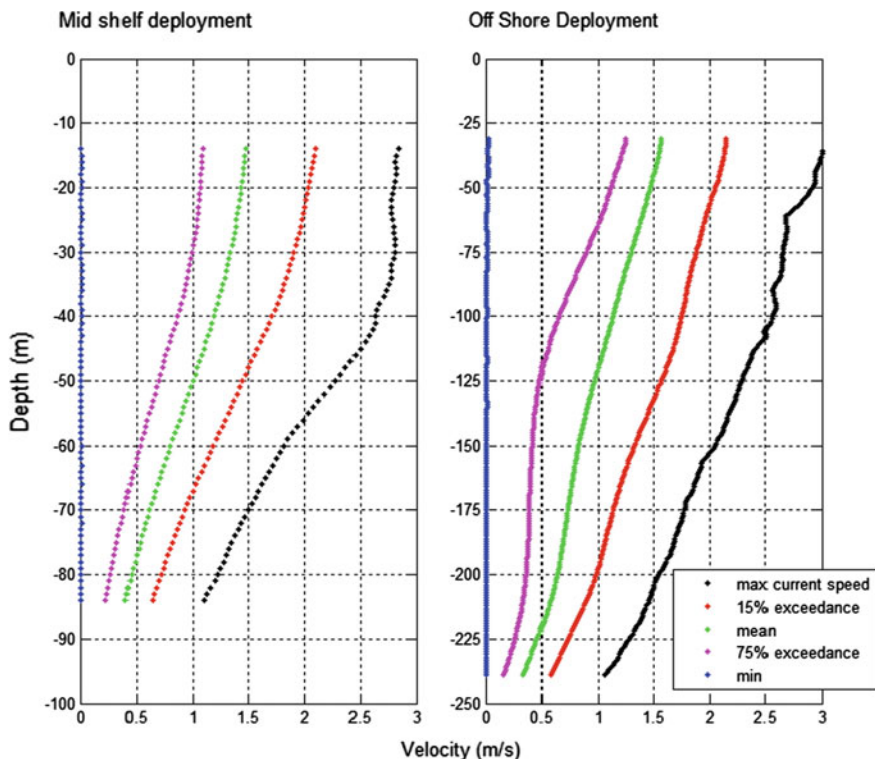


Fig. 7 Current velocity magnitude (m/s) ADCP minimum (blue), 75% (magenta), mean (green), 15% (red), and maximum (black) flow speeds at the mid-shelf (left-hand figure) and offshore (right-hand figure) locations (Meyer and Van Niekerk 2016)

array because all power production will stop during the presence of a Natal Pulse. Three other time periods of low velocity magnitude seen in these figures indicate the presence of eddies in the current core—during February 2012, May 2012, and October 2012. These eddies did not persist as long as the occurrence in April 2013, but such events add to the variability of the current and lower the availability of the current.

Rouault and Penven (2011) found an average of 1.6 Natal Pulses travel down the East Coast of South Africa annually. The data set evaluated here is 18 months long and has only one distinct occurrence present that can result in a more optimistic capacity factor for this period than in an average year. This shows that the measured in situ data sets cannot be used in isolation to quantify the performance of the current, but need to be compared to data sets that cover a longer period of time (10 years or more) to ensure correct trends are observed, and this can be achieved by using remote-sensing data.

Figures 10 and 11 show the velocity magnitude distribution and cumulative frequency of occurrence at the 30 and 50 m depths for each of the locations. In both

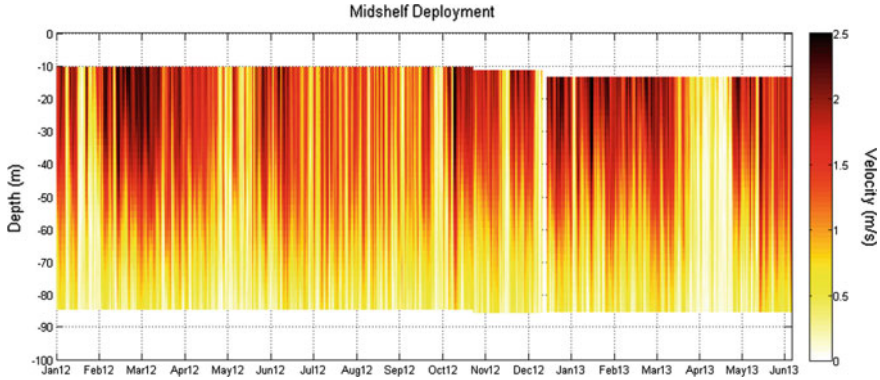


Fig. 8 Temporal plot at the mid-shelf location. Time versus depth with the colour scale indicating current speed (m/s) (Meyer and Van Niekerk 2016)

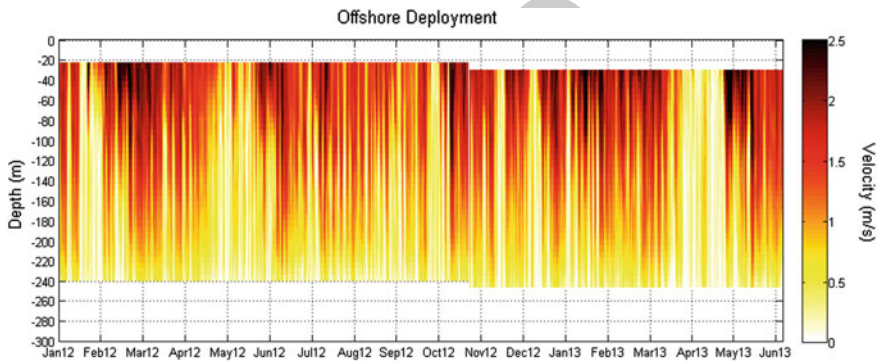


Fig. 9 Temporal plot at the offshore location. Time versus depth with the colour scale indicating current speed (m/s) (Meyer and Van Niekerk 2016)

451 Figs. 10 and 11, in the Frequency of Occurrence plot, two distinct peaks are seen:
 452 the first is low velocity magnitude peak, indicating the velocity magnitude distribu-
 453 tion during the presence of a Natal Pulse or weekly eddies, and the second occurs
 454 when no such phenomena are present. The second peak tends to the bell shaped
 455 curve of a normal distribution curve, but is skewed to the left by low velocity
 456 magnitude values. This observed distribution must be noted when the mean velocity
 457 magnitude or mean power density is evaluated throughout the water column,
 458 because if the periods when Natal Pulses are present are treated as maintenance
 459 periods and are thus excluded, then the average velocity magnitude or power
 460 density will be higher than represented. However, as seen in Figs. 10 and 11, there
 461 are periods of low velocity magnitude that do not persist as long as Natal Pulses, but
 462 they will negatively affect potential power production and cannot be discounted.

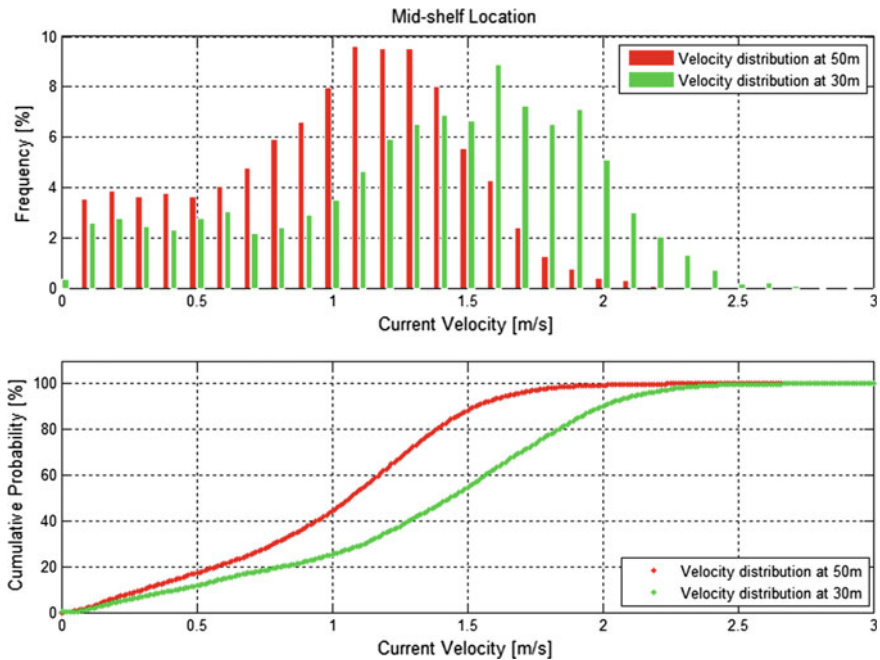


Fig. 10 Velocity magnitude distribution at the mid-shelf location (Meyer and Van Niekerk 2016)

463 The typical cut-in speed of marine turbines is between 0.5 and 1.0 m/s (Meyer
 464 and Van Niekerk 2016). If the velocity magnitude distribution is compared to these
 465 velocity magnitude values for both the mid-shelf and offshore location, one notes
 466 that the low velocity magnitude peak present in the full distribution curve will result
 467 in non-operational turbines.

468 In Figs. 10 and 11, the shift in the histogram bars towards the higher velocities
 469 for the shallower measurement highlights the difference in velocity magnitude seen
 470 at the 30 m depth compared to the 50 m depth. There is less of a difference between
 471 the velocities at the 30 and 50 m depths at the offshore location due to the deeper
 472 penetration of the current core at this site and lesser impact of seabed drag on the
 473 current. Furthermore, velocities at a 60 m water depth at the offshore location are
 474 comparable to the velocities at a 20 m depth at the mid-shelf location. This is
 475 important to note because deploying and mooring a turbine array at a sea bed depth
 476 of 255 m may prove to be challenging. Figure 8 through Fig. 11 reiterate the
 477 importance of mooring the turbine array as close to the surface as possible for
 478 maximum power output.

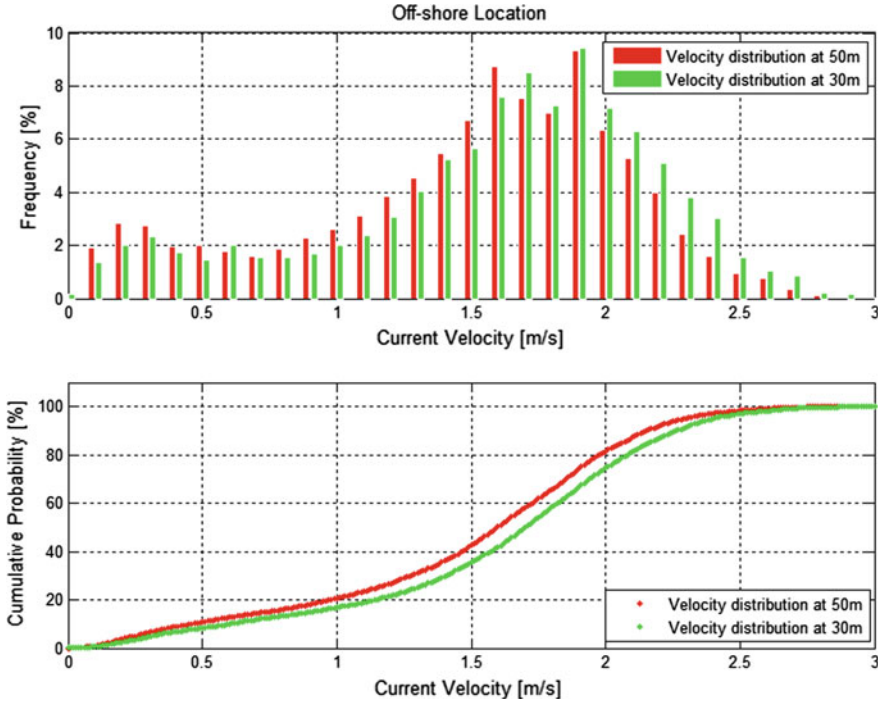


Fig. 11 Velocity magnitude distribution at the offshore location (Meyer and Van Niekerk 2016)

Power Density

The power density of a fluid stream across a unit cross section is given by:

$$P = \rho \frac{1}{2} v_{ins}^3 \quad (1)$$

where ρ is the density of the fluid and v_{ins} is the instantaneous velocity magnitude of the fluid stream.

The mean power density versus depth is plotted in Fig. 12. As noted in the velocity magnitude analysis, the power density at 20 m at the mid-shelf deployment ($2,265 \text{ W/m}^2$) is similar to that at 60 m at the offshore deployment ($2,180 \text{ W/m}^2$). At the 30 m water depth, the mean power density is $1,857$ and $2,866 \text{ W/m}^2$ at the mid-shelf and offshore locations, respectively. The power density at the offshore location is 1.5 times greater than the power density at the mid-shelf location at the 30 m water depth. At the 50 m water depth, the mean power density is 813.6 and $2,440 \text{ W/m}^2$ at the mid-shelf and offshore locations, respectively. This results in the power density at the offshore location being three times larger than that of the mid-shelf deployment at the 50 m water depth. When comparing these values with

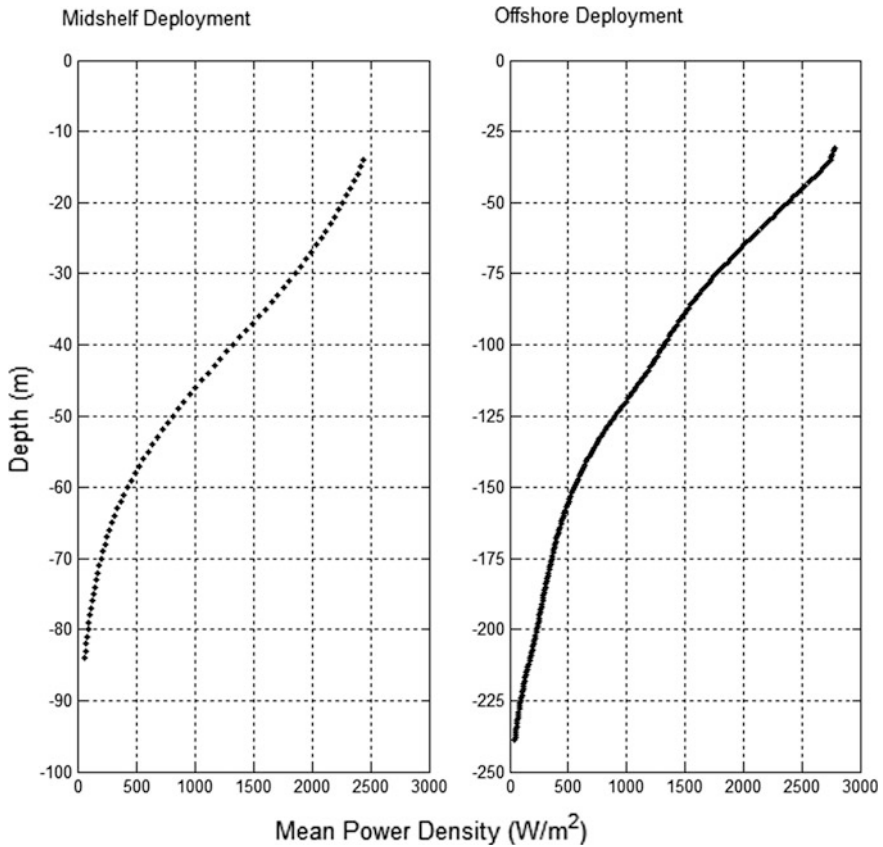


Fig. 12 Mean power density (W/m^2) (Meyer and Van Niekerk 2016)

496 the current velocity magnitude at the same depths, the cubed relationship between
 497 power and velocity magnitude is highlighted.

498 *Directional Analysis*

499 The current direction at each location is described using directional roses plotted at
 500 depths of 80, 50, and 30 m in Fig. 13. When the mid-shelf and offshore locations
 501 are compared a slight shift in the predominant current direction is seen as the
 502 current approaches the shore.

503 At the offshore location, the predominant current direction is approximately 195°
 504 from North where at the mid-shelf location, the predominant current direction is
 505 210° from North. This directionality shows that the current flows in a general
 506 south-westerly direction with onshore components.

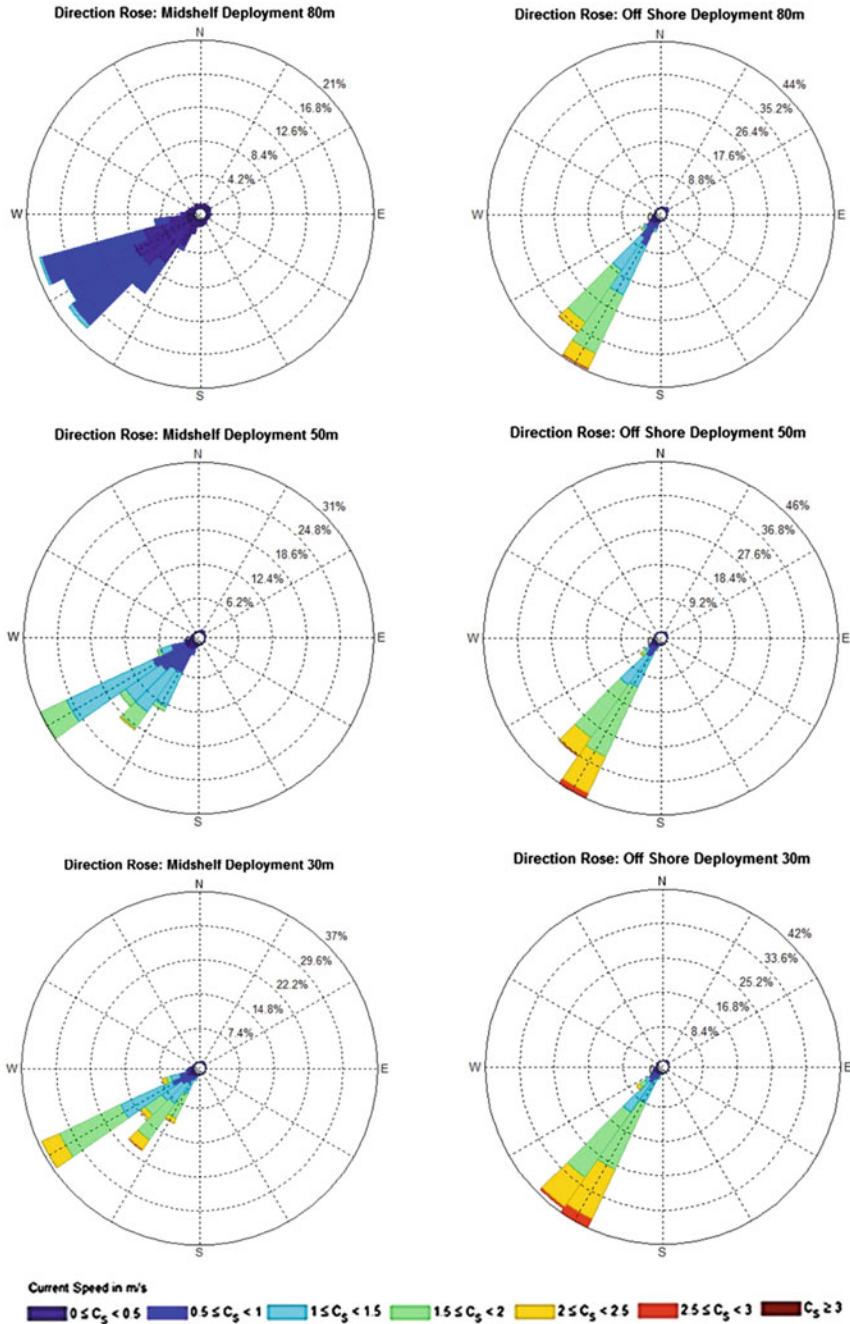


Fig. 13 Mid-shelf location (left) and offshore location (right): current directional roses at the 80 m (top), 50 m (centre), and 30 m (bottom) water depths (Meyer and Van Niekerk 2016)

At the mid-shelf location, at the 80 m water depth, onshore directional tendencies are seen, whereas at the 50 and 30 m water depths, the directionality ranges between 195° and 210° from North. The current directionality is more constant at the offshore location where only two predominant directions are seen, namely 195° and 200° from North, compared to the mid-shelf deployment that possesses five distinct directional components. This indicates the presence of the core at the offshore location, where the more swift flowing waters reduce the variability in the direction of the current.

The directional roses do not show directionality when the velocity magnitude is zero, but the near-zero velocity magnitude components can be seen to ring the centre of the rose, indicating that during eddies or Natal Pulses the directionality of the current is no longer in the south-westerly direction and current reversals take place.

Figure 14 illustrates the relationship of the standard deviation of direction and the percentage of current reversals with depth below the sea surface. The standard

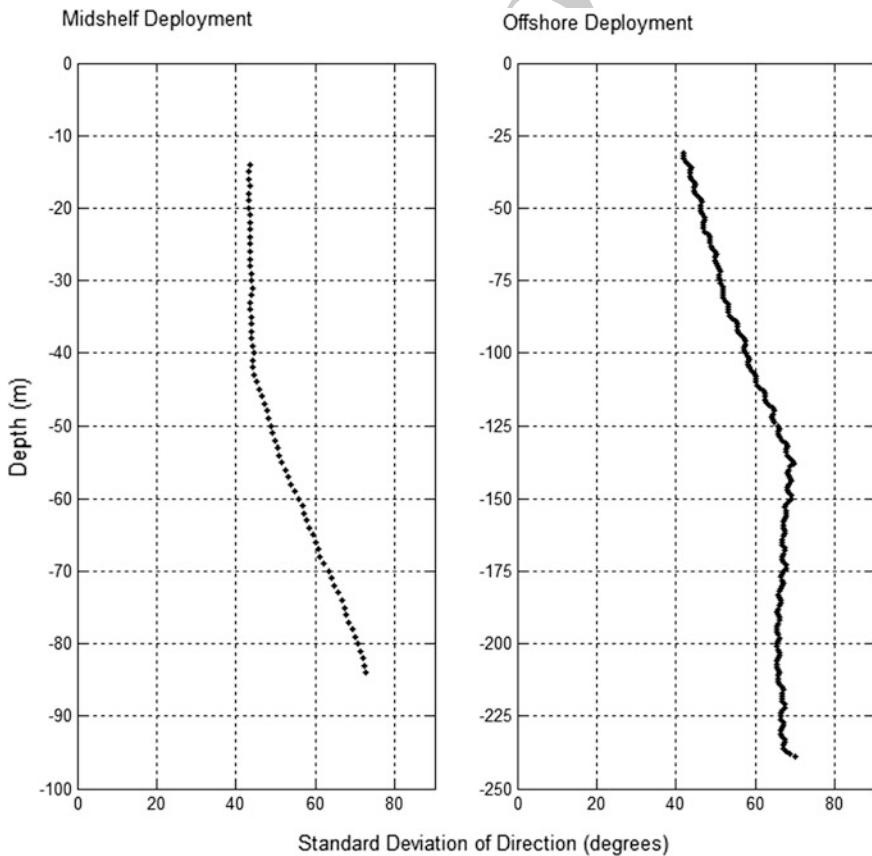


Fig. 14 Standard deviation of flow direction in degrees (Meyer and Van Niekerk 2016)

521 deviation of the current's direction increases with depth in the upper water column
522 as seen in both mid-shelf and offshore locations. In the offshore location, the
523 variability stabilises below a depth of 137 m. At the 30 m depth, the standard
524 deviation is 43.98° and 40.08° for the mid-shelf and offshore locations, respec-
525 tively. At a depth of 50 m, the standard deviation is 48.66° and 44.85° for the
526 mid-shelf and offshore locations, respectively. This variability shows that the
527 chosen turbine must be able to adapt to the change in flow direction in order to
528 achieve a maximum power output.

529 **Technical and Environmental Considerations**

530 *Technology Considerations*

531 The magnitude of practically extractable power depends on the technology used to
532 harness the current's energy and the power density at which this technology can be
533 deployed. The ocean energy industry as a whole is still immature; ocean current
534 energy technology readiness levels range between TRL 1 and TRL 5 (Mofor et al.
535 2014). At the time of this study, no ocean current turbines are operating at a
536 commercial scale for energy extraction.

537 From the results of the current magnitude and directional analysis, it is estab-
538 lished that the required technology needs to operate in a flow range of 0.6 and 2 m/s
539 with the mean velocity magnitude occurring between 1 and 1.5 m/s. Further, this
540 technology must be adaptable to change in current direction and must be able to
541 survive the presence of a Natal Pulse that results in a period of zero velocity
542 magnitude.

543 Of the technology developers developing turbines for tidal applications, Mine-
544 sto, has expressed interest in adapting the Deep Green 500 kW turbine for ocean
545 current applications with a specific focus on the Gulf Stream (reNews 2014). The
546 Minesto technology holds promise with a design that accelerates the flow velocity
547 through the use of relative motion as the turbine flies through the water in a figure
548 eight pattern. The Minesto Deep Green 500 kW turbine is a tethered turbine with a
549 rated operating speed of 1.6 m/s, cut-in speed of 0.5, and cut-out speed of 2.5 m/s
550 (Minesto 2015). These parameters indicate the suitability of the Minesto Deep
551 Green turbine for deployment in the Agulhas Current.

552 Another tethered turbine, the Aquantis 2.5 MW C-Plane, has been specially
553 designed to operate in ocean currents (specifically the Gulf Stream) and has a rated
554 speed of 1.6 m/s, which indicates the potential suitability of this device for
555 deployment in ocean current applications (Ecomerit Technologies 2012). However,
556 at the time of this study, no sea trials have been carried out on the C-Plane, so the
557 success of the device is still to be verified. Similarly, IHI Corporation and Toshiba
558 are currently developing a tethered turbine for deployment in the Kuroshio Current.

559 This device is still in the simulation phase and construction is yet to begin (IHI
560 Corporation 2015).

561 To compare the variability of the Agulhas Current to other renewable energy
562 resources, a suitable turbine is selected and a capacity factor is obtained from the
563 practically extractable power. Array configuration and spacing are not considered in
564 this research and the capacity factor of a single turbine is presented. The capacity
565 factor is described by the following expression:
566

$$C_f = \frac{\sum_{i=1}^N \text{Powerproduced}}{\sum_{i=1}^N \text{Turbineratedpower}} \quad (2)$$

568 where N is the total number of time steps over which the capacity factor is
569 calculated.
570

571 The theoretical power produced by the turbine is found by using the published
572 power curve (found in Minesto 2011); a polynomial equation is developed to follow
573 this power curve of the turbine using instantaneous velocity magnitude as the input
574 and instantaneous power as the output. For the Minesto turbine that travels through
575 a range of depths, this calculation method makes use of the instantaneous velocity
576 magnitude at one depth, and thus, with the observed decreasing vertical velocity
577 magnitude profile, this method of calculation has the potential to overestimate the
578 total energy output from the system. Furthermore, as outlined by Hass et al. (2013),
579 a single turbine has little to no effect on the upstream characteristics of the current,
580 but a large number of devices can block the flow and reduce the current velocity,
581 and hence reduce the generated power from each device. Thus, it is noted that this
582 methodology cannot be extrapolated to an array of turbines, but rather can be used
583 as a comparative method to identify an energetic site.

584 The theoretical capacity factors at the mid-shelf and offshore location for the
585 deployment of one Minesto Deep Green 500 kW turbine is presented in Table 5.
586 Table 6 presents the findings from the 500 kW Deep Green turbine that has a rated
587 speed of 1.6 m/s and an optimal operating range of 1.4–2.2 m/s. Similar to the wind
588 turbine industry, the economics of the availability of power versus the magnitude of
589 the power produced must be weighed against one another to find the best-suited
590 turbine. Table 6 shows the theoretical power output and specific yield from the
591 500 kW Minesto turbine.

592 Upon examination of Table 5, the capacity factor for the offshore location is
593 significantly higher than the mid-shelf location; there is only a 6% drop in capacity

Table 5 Found capacity factor for the Minesto 500 kW turbine

Minesto 500 kW deep green rated speed of 1.6 m/s		
Depth (m)	Mid-shelf location (%)	Offshore location (%)
30	62	74
50	37	68

Table 6 Theoretical power output at the 30 m depth

	Minesto 500 kW deep green rated speed of 1.6 m/s	
	Annual yield (MWh/annum) (MWh)	Specific yield (kWh/yr-kW installed) (kWh/kW)
Mid-shelf location	2,708	5,416
Offshore location	3,258	6,515

594 factor between the 30 and 50 m deployment depths. At the mid-shelf location, a
595 25% drop in capacity factor is seen between the 30 and 50 m deployment depths.
596 Because the mid-shelf location is situated at the edge of the Agulhas Current, the
597 core does not penetrate as deeply as at the offshore location, which results in a drop
598 in velocity that is amplified by the cubed power velocity relation and the subsequent
599 drop in capacity factor.

600 When comparing the found capacity factors at both locations to the values of
601 other renewable energy resources, the Agulhas Current fares well. Desktop analysis
602 by Kritzinger (2015), in collaboration with the South African. Department of
603 Energy's Independent Power Producer office, approved for publication in 2014,
604 found that for the South African wind resource, the capacity factor for the
605 under-construction or installed wind farms greater than 80 MW ranges from 30 to
606 45%. If the turbines are installed at 50 m or shallower depths, the found capacity
607 factors are greater than those generated by wind farms for both analysed turbines.
608 A typical capacity factor found for tidal energy extraction ranges from 20 to 30%,
609 and for wave energy extraction devices, it ranges from 15 to 22% (Boyle 2012). The
610 found capacity factors of the Agulhas Current point to a more constant resource in
611 comparison to other renewable energy resources, which indicates a possible con-
612 tribution to the base-load supply of electricity.

613 For the 500 kW turbine, the annual electricity production at the offshore location
614 is 3.26 GWh and at the mid-shelf location it is 2.71 GWh. Although the capacity
615 factor and the specific yield of the offshore site is higher than that of the mid-shelf
616 location, the economics of the longer sea cable and increased mooring challenges
617 must be taken into consideration when deciding on an optimal deployment location.

618 The closest developed technology to that of ocean current turbines is the tech-
619 nology developed to harness tidal stream energy. The rated operating speed of the
620 stationary (gravity or pile mounted) horizontal axis turbines is greater than 2.5 m/s,
621 so these turbines will perform poorly if deployed in the Agulhas Current. Further,
622 the pile mounting or gravity base will prove problematic due to the mooring depth
623 at energetic ocean current sites. Tethered turbines still require development to be
624 optimally deployed in the Agulhas Current; however, Minesto has gained support
625 from the Welsh government and plans to deploy a 10 MW array by 2019 at
626 Holyhead Deep off the coast of Anglesey (Minesto 2015), which indicates progress
627 towards a commercial industry. The turbines used in the analysis are designed

628 specifically for tidal applications, so the turbine chosen for the Agulhas Current
 629 conditions will need to be optimised to maximise the turbine capacity factor and
 630 produced energy.

631 The practically extractable power depends not only on the selected power
 632 take-off technology and resource velocity magnitude and directionality, but also is
 633 on a number of other factors, as discussed below.

634 *Geotechnical and Mooring Considerations*

635 With respect to current magnitude and direction, the study results indicate that a
 636 strong and constant flow of seawater takes place at deeper locations because the
 637 current core lies approximately above the 200 m bathymetry line at 28.831 E and
 638 32.507 S. However, the deeper the sounding depth, the larger will be the concerns
 639 surrounding the mooring challenges and the drag forces on the turbine tether in
 640 order to moor the turbine hub at 30 m below the surface. A stronger and more
 641 advanced mooring system will be required at deeper locations, and the economics
 642 of higher power production versus the cost of a more robust mooring system must
 643 be considered.

644 Most experience in such applications is related to the mooring of tidal energy
 645 extraction devices and this mooring takes place in water depths of less than 100 m.
 646 Because there is no oil drilling activity in the area off the eastern South African
 647 coast, practical engineering experience gained from working in the required water
 648 depths is lacking. When working in water depths of 100 m or less some of the
 649 lessons learned from the tidal industry will be transferable, but when working in a
 650 tidal resource there is a period of slack water as the tide changes between ebb and
 651 flow. The constant flow of the current may prove to be challenging during the
 652 deployment and maintenance of ocean current power plants.

653 To ensure the successful mooring of turbines within the Agulhas Current, the
 654 engineering constraints related to the environment need to be well understood. For
 655 example, the sedimentary and geotechnical properties of the seabed relative to
 656 mooring need to be considered. Limited information is available about these
 657 characteristics and properties of the subsurface ocean. Documentation of ocean bed
 658 topography along the southeast coast of South Africa occurred in the late 1970s and
 659 the information presented here is based on the associated maps and findings.

660 Figure 15 shows a schematic diagram of the shelf section between the latitudes
 661 of 28 and 34 S. The region of focus (Sections B and C in Fig. 15) is the outer-shelf
 662 region that is dominated by the current. The Agulhas Current dictates the sedi-
 663 mentary transport in this region. Here, the presence of shifting subaqueous dunes
 664 and relict gravels is seen. Dune heights of up to 8 m, lengths of 200 m, and dune
 665 field widths of a minimum of 10 km have been recorded. The outer-shelf gravels
 666 consist of relict sediments produced during the early Flandrain transgression by
 667 reworking of fossil algal reef bioherms (Flemming 1978). There is a distinct change
 668 in bed form type between the inner shelf and outer shelf, which consist of relict

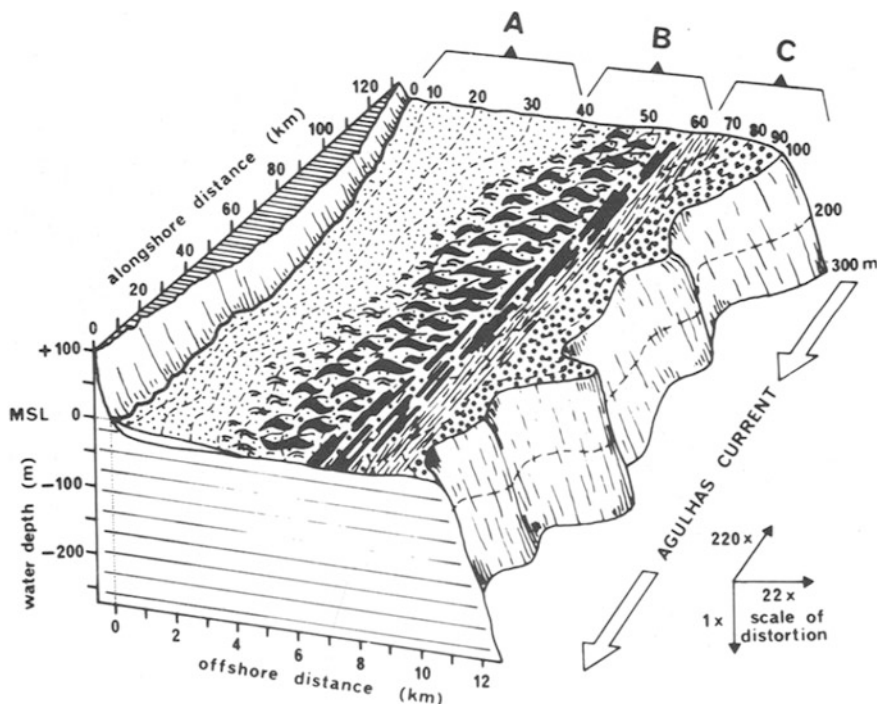


Fig. 15 Schematic block diagram of the shelf section summarising the sedimentary and structural characteristics of the ocean floor topography (Flemming 1980)

669 carbonate facies. The continental shelf has a very steep slope ($\sim 12^\circ$ gradient) and is
 670 dissected by numerous submarine canyons. The outer-shelf region consists of
 671 current-generated bed forms such as sand streamers, dunes, and an exposed gravel
 672 pavement (Flemming 1980).

673 The shifting dunes can be problematic because cabling running ashore can be
 674 exposed, thereby increasing the risk of scour and requiring more frequent main-
 675 tenance of the cabling. The presence of the dunes will also increase the amount of
 676 dredging that has to be done before bedrock is reached. These dunes are a con-
 677 tinuous feature along the southeast margin of the African continent and thus will be
 678 encountered continuously along the coast.

679 An array of turbines will be tethered and anchored to the sea bed. The concerns
 680 surrounding this mooring method will be similar to those in other unidirectional
 681 currents that have one main loading direction where vortices and vortex shedding
 682 may be problematic. The device will have to be robust and designed to withstand
 683 geological and environmental extremes while keeping the sophisticated equipment
 684 afloat, thus the anchoring foundation must be designed for dynamical loading. The
 685 anchors must be designed to resist high cyclic lateral loads and have good scour
 686 protection on the tethering cable (Dean 2010).

687 Another phenomenon within the Agulhas Current is the presence of “Giant
 688 Waves” that are unpredictable and have the ability to break large ships in two
 689 (Lutjeharms 2006). These waves occur in the core of the current at the landward
 690 border, the same position being investigated for device deployment. Although the
 691 energy extraction devices will be located at least 20 m below the surface, such
 692 extreme conditions must be taken into account when addressing maintenance
 693 concerns and the fatigue loading in the device and mooring system.

694 Very little experience has been gained with respect to mooring considerations in
 695 this region, so extensive geotechnical surveys will have to be carried out if ocean
 696 current energy becomes a reality.

697 *Commercial Fishing Activities*

698 Figure 16 shows areas of importance to the fisheries industry. The map shows a
 699 cost–benefit analysis indicating the zones of high yield. The area of interest for
 700 current turbine development lies between East London and Port St John’s, and from
 701 Fig. 16, it can be seen that this is not a prime area for fishing. This finding is
 702 positive because placing a turbine array in this area will help unlock the economic
 703 potential of the ocean in this region without interfering with other economic
 704 activities or ocean users. This is a preliminary finding; the site-specific effect of the
 705 turbine array on commercial and subsistence fish farmers will need to be determined
 706 by conducting an environmental impact assessment.

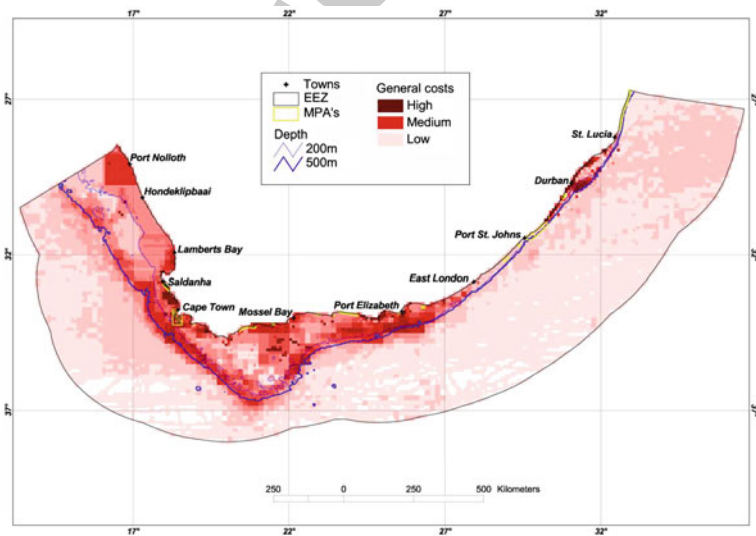


Fig. 16 Map showing the cost benefit to the fisheries industry. The darker areas are of greater importance to the industry in both benthic and pelagic respects (Sink et al. 2011)

Shipping Routes

The shipping route down the east coast of South Africa is an important trade route as illustrated in Fig. 17 by the number of journeys made during a one-year period. The establishment of a turbine array must not hinder this economic activity, and the appropriate depth below the surface must be established. Although the deployment depth of the turbines will take heed of ship wakes, exclusion zones may have to be considered with respect to ship anchoring concerns in the region of turbine deployment.

Existing Infrastructure that Can Consume the Generated Energy

A schematic of the existing Eskom substations is seen in Fig. 18, which indicates the distances from the ADCP deployment locations (mid-shelf and offshore locations indicated by white circles). The mid-shelf site is located 14 km from the shore and 30 km from the nearest medium voltage station. The offshore site is 18 km from shore and 30 km from the nearest medium voltage station. This indicates that there is existing infrastructure to make use of the generated electricity, but an economic analysis must be carried out to determine whether the increased power generated at the offshore location justifies the increase in sea cabling length. The

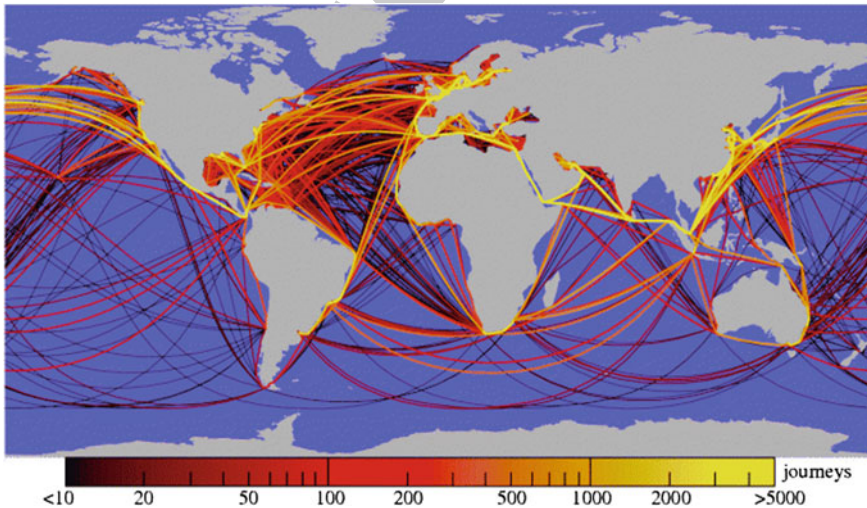


Fig. 17 Trajectories of all cargo ships bigger than 10,000 GT during 2007 (Kaluza et al. 2010)

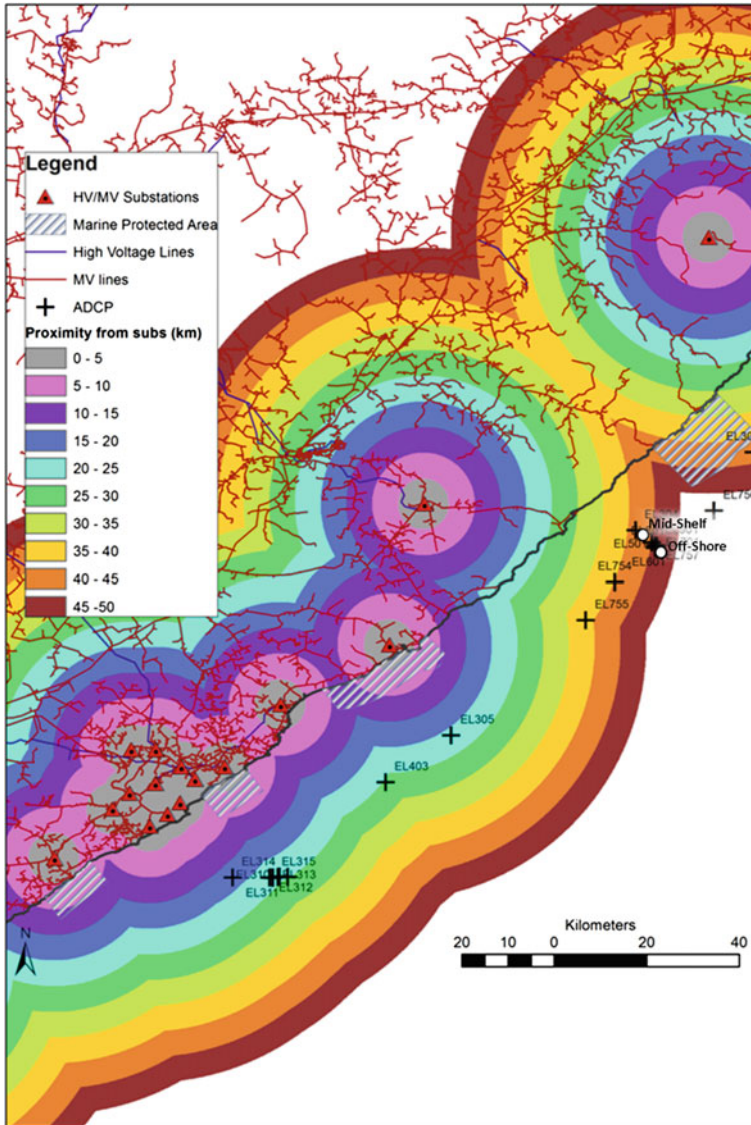


Fig. 18 Position of existing Eskom substations in the region of interest (Meyer et al. 2013)

725 distances from the deployment sites to the nearest substation are significantly longer
 726 than those seen for tidal sites, but are comparable to offshore wind sites. For
 727 offshore wind sites, subsea AC cabling is used for projects located up to approxi-
 728 mately 60 km offshore (Norton et al. 2011).

729

Environmental Impact

730

731

732

733

734

735

736

737

738

739

The closest existing marine protected area lies 15 km north of the analysed sites. No marine protected areas lie between the selected sites and the closest harbour located on the coast is Port Elizabeth, 350 km southwest of the chosen sites. The positions of the existing and proposed marine protected areas along the South African coastline are seen in Fig. 19. The closest economic hub in this area is East London, which lies south of the analysed sites; thus, no cabling or vessels required for the deployment and maintenance of the devices will pass through marine protected areas. It is also encouraging to notice that the proposed marine protected areas will not cause obstacles in this regard. Furthermore, the chosen turbines are shrouded, which decreases the impact of these devices on marine mammals.

740

741

742

743

744

745

746

747

748

749

750

On a larger scale, the environmental impact on the meridional overturning circulation of placing turbines that extract energy from the Agulhas Current has not yet been investigated and the maximum size of a potential power plant is yet to be established. In 2007, the Bureau of Ocean Energy Management published an Environmental Impact Statement (U.S. Department of the Interior Minerals Management Service 2007) in which the effects of deployment of ocean current turbines in the Gulf Stream are considered. The impacts will depend on the technology and array configuration chosen, but typical impacts include reduction in current velocity and energy and possible reduction in wave height in the vicinity of the devices (U.S. Department of the Interior Minerals Management Service 2007). Reduction of wave height will be localised, but the reduction in current energy can affect larger

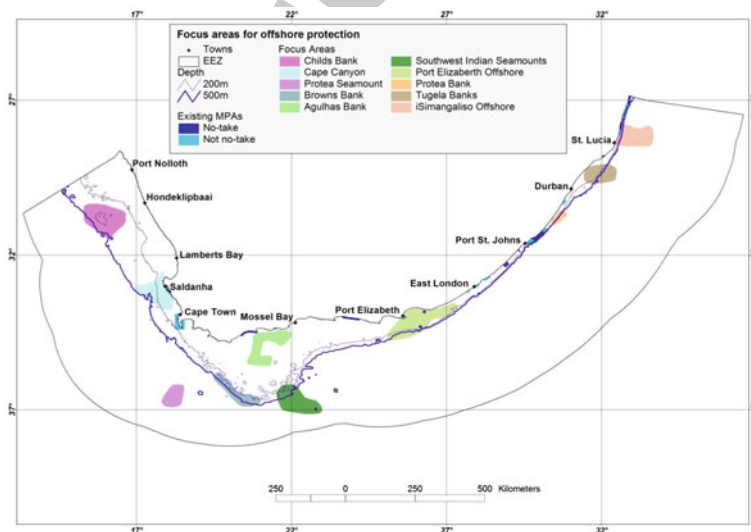


Fig. 19 Existing and proposed marine protected areas around the South African coast (Sink et al. 2011)



751 systems—namely weather patterns and the interactions of current with nearshore
752 waters.

753 Using a depth-averaged 2D equation model, Haas et al. (2013) examined the
754 effects of placing an array of turbines in the Gulf Stream. For a limited turbine
755 array, the impact of turbines was found to be primarily confined in the turbine
756 regions with negligible far-field effects. However, as the turbine region increases
757 the region with reduced flow grows accordingly and leads to a reduced flow rate. If
758 the turbine region extends across the core of the Gulf Stream, the energy extraction
759 from the turbines can slow the flow universally across the entire basin. Such
760 impacts within the Agulhas Current will need to be determined through large-scale
761 ocean modelling. The impacts of ocean current turbine systems can be limited by
762 restricting the quantity of energy extracted from the current and maximising the
763 efficiency of the systems deployed. If such mitigations are put in place, this envi-
764 ronmental challenge should not result in the discontinuation of ocean current
765 projects.

766 *Regulatory Environment*

767 South Africa has a well-established National Environmental Management: Inte-
768 grated Coastal Management Act (2008) (ICMA) that regulates the activities along
769 its coastline. Prior to any construction on the coastline, an environmental impact
770 assessment will need to be carried out in accordance with this Act. However, there
771 is a lack of Marine Spatial Planning (MSP) within the Exclusive Economic Zones
772 of South Africa to regulate marine usage by the various stakeholders in the marine
773 environment. The launch of Operation Phakisa has seen the establishment of a
774 formal MSP process for South Africa. The MSP focus areas are aquaculture,
775 mining, shipping, fisheries, and conservation (Marine Protection Services and
776 Governance 2014). Renewable energy has been excluded from this plan, and this
777 can result in uncertainty surrounding the consenting process for marine renewable
778 energy projects.

779 Other formal permits that will need to be considered in order to obtain consent
780 for a marine renewable energy project include those associated with the National
781 Environmental Management Biodiversity Act, Sea Birds and Seals Protection Act,
782 and National Energy Regulator of South Africa Electricity Regulation Act. This is
783 not necessarily a comprehensive list because each project's permitting will need to
784 be approached on a site-by-site basis.

785 From the preliminary analysis of other contributing factors, no one factor will
786 cause such a project to be a no-go. The economics of such an endeavour are still a
787 challenge and the environmental concerns will need to be addressed so that
788 renewable energy stakeholders become well-established and welcomed users of the
789 marine environment.

Conclusion About the Best Site

Through the analysis of ADCP, GlobCurrent, and HYCOM data sets along the eastern South African coastline, an area of swift, stable flow in the Agulhas Current has been identified. This area is approximately 100 km northeast of East London, the closet economic hub. One mid-shelf and one offshore site in this area were analysed, and the offshore site was found to be more energetic with higher velocities and reduced directional variability. The mean velocity found at the 30 m depth at the offshore location is 1.59 m/s, and the mean velocity at the mid-shelf location is 1.34 m/s. Ideally, a turbine will operate at a rated speed within this velocity magnitude range.

Unique challenges for exploiting this resource for energy generation exist, including the irregular occurrence of large Agulhas Current meanders (known as Natal Pulses). The comparison between GlobCurrent and HYCOM data and in situ ADCP data was used to determine if this variability can be captured remotely. PCA showed that the GlobCurrent product shows a weaker Agulhas Current with less variability than indicated by the in situ data, and the HYCOM product shows more accurate Agulhas Current velocities but very little variability in the current. Comparison of the ADCP, GlobCurrent, and HYCOM data spectra indicates that the satellite-derived product is able to capture the correct levels of variability in terms of the inverse energy cascade of processes in the ocean, while the modelled data show some limitations in this regard. However, upon closer examination, it is evident that both GlobCurrent and HYCOM data sets only adequately represent scales of variability at the monthly time scale. This latter fact places a significant limiting factor on using these data for prediction to inform stakeholders and highlights the need for further development and improvement of these products.

Nevertheless, in the absence of a spatial and temporally coherent ocean observation system for the Agulhas Current, these data provide useful insights into the modes of variability in the Agulhas Current and their implications for energy production. With the aid of satellite measurements, the presence of Natal Pulses have been found to be predicted approximately 15 days prior to their occurrence at the identified energetic site if tacked from a location higher up the coast. It should be noted, however, that the reduced correlation between in situ and satellite data at the weekly to 10-day time scale may decrease the accuracy of such predications. This prediction will help in minimising the effects of this phenomenon because such periods of no production can be used for scheduled maintenance, and grid planners will have warning enough to mobilise other forms of power generation.

To reduce the barrier of entry into the ocean energy market in South Africa, the challenges facing remote-sensing and assimilative modelling data need to be addressed. There is a critical need for the predictive ocean modelling and satellite remote-sensing community to develop the capabilities to resolve the high spatial-temporal resolution processes needed for accurate characterisation of ocean current energy potential. The new Sentinel series satellites recently launched by the European Space Agency may provide the high-resolution data satellite required.

833 Regional modelling and data assimilation efforts such as those detailed by
834 Backeberg et al. (2014) are critical for achieving improved predictive skill in the
835 Agulhas Current in particular. The open access nature of these data sets is instru-
836 mental in opening the market to future developers as well as in reducing future
837 monitoring and operational costs. If the region of interest is accurately mapped at a
838 high resolution, this knowledge can be used to inform MSP policies so that marine
839 energy extraction activities can be taken into consideration and further advance the
840 industry.

841 Although a number of engineering and financial issues challenge deployment of
842 a turbine array in the Agulhas Current, if the resource is paired with the correct
843 turbine, the estimated capacity factors compare well with other renewable energy
844 resources; thus, this current holds potential to make a significant contribution to the
845 South African electricity grid.

846 **Acknowledgements** The authors would like to acknowledge the South African national utility
847 Eskom for making available the data, without which this research would not have been possible.
848 Dr Backeberg acknowledges joint support from the Nansen-Tutu Centre for Marine Environmental
849 Research, Cape Town, South Africa; the Nansen Environmental and Remote Sensing Center,
850 Bergen, Norway; and the South African National Research Foundation through the Grants 87698
851 and 91426. This work has also received a grant for computer time from the Norwegian Program
852 for supercomputing (NOTUR project number nn2993 k). Special thanks to Dr Julie Deshayes for
853 her input and guidance in analyzing the spectra. Both the GlobCurrent and HYCOM data used in
854 this study are freely available online at <http://www.globcurrent.org> and hycom.org, respectively.
855 GlobCurrent products are available for free thanks to European Space Agency funding under
856 GlobCurrent DUE project A0/1-7472/13/I-LG.

857 References

- 858 Backeberg, B. C., Counillon, F., Johannessen, J. A., et al. (2014). *Ocean Dynamics*, 64, 1121.
859 doi:10.1007/s10236-014-0717-6.
- 860 Beal, L. M., & Bryden, H. L. (1999). The velocity and vorticity structure of the Agulhas Current at
861 32 S. *Journal of Geophysical Research*, 104(C3), 5151–5176.
- 862 Biastoch, A., Lutjeharms, J. R. E., Böning, C. W., & Scheinert, M. (2008b). Mesoscale
863 perturbations control inter-ocean exchange south of Africa. *Geophysical Research Letters*, 35
864 (L20602).
- 865 Boyle, G. (2012). *Renewable energy* (3rd ed.). Oxford: Oxford University Press.
- 866 Bryden, H. L., Beal, L. M., & Duncan, L. M. (2005). Structure and transport of the Agulhas
867 Current and its temporal variability. *Journal of Oceanography*, 61, 479–492.
- 868 Chang, Y.-C., Chu, P. C., & Tseng, R.-S. (2015). Site selection of ocean current power generation
869 from drifter measurements. *Renewable Energy*, 80, 737–745. doi:10.1016/j.renene.2015.03.
870 003.
- 871 Chen, F. (2010). Kuroshio power plant development plan. *Renewable and Sustainable Energy*
872 *Reviews*, 14(9), 2655–2668. doi:10.1016/j.rser.2010.07.070.
- 873 Cummings, J. A. (2005). Operational multivariate ocean data assimilation. *Quarterly Journal of*
874 *the Royal Meteorological Society, Part C*, 131, (613), 3583–3604.
- 875 Dean, E. (2010). *Offshore geotechnical engineering*. London: Thomas Telford Limited.
- 876 Dohan, K., & Maximenko, N. (2010). Monitoring ocean currents with satellite sensors.
877 *Oceanography*, 23(4), 94–103. doi:10.5670/oceanog.2010.08.

- 878 Ducet, N., Le Traon, P.-Y., & Reverdin, G. (2000). Global high-resolution mapping of ocean
879 circulation from TOPEX/Poseidon and ERS-1 and -2. *Journal Geophysical Research*, *105*,
880 19477–19498.
- 881 Duerr, A. S., & Dhanak, M. R. (2012). An assessment of the hydrokinetic energy resource of the
882 Florida current. *IEEE Journal of Oceanic Engineering*, *37*(2), 281–293.
- 883 Ecomerit Technologies, (2012). Aquantis [Online]. <http://www.ecomeritech.com/aquantis.php>.
884 [2015, February 7].
- 885 Ekman, V. W. (1905). On the influence of the Earth's rotation on ocean currents. *Archives of*
886 *Mathematics, Astronomy, and Physics*, *2*(11), 1–52.
- 887 Flemming, B. (1978). Underwater Sand Dunes along the Southeast African continental
888 Margin-Observations and implications. *Marine Geology*, *26*, 177–198.
- 889 Flemming, B. (1980). Sand transport and bedform patterns on the continental shelf between
890 Durban and Port Elizabeth (Southeast African Continental Margin). *Sedimentary Geology*, *26*,
891 179–205.
- 892 Fox, D. N., Teague, W. J., Barron, C. N., Carnes, M. R., & Lee, C. M. (2002). The modular ocean
893 data assimilation system (MODAS). *Journal of Atmospheric and Oceanic Technology*, *19*,
894 240–252.
- 895 Gründlingh, M. L. (1983). On the course of the Agulhas Current. *South African Geographical*
896 *Journal*, *65*, 49–57.
- 897 Haas, K. et al. (2013). Assessment of Energy Production Potential from Ocean Currents along the
898 United States Coastline, Atlanta.
- 899 IHI Corporation, Power Generation Using the Kuroshio Current, (n.d.). Retrieved November 26,
900 2015 from [http://www.ihico.jp/var/ezwebin_site/storage/original/application/
901 149ee9de3149aba2e1215fd5f9cd46ec.pdf](http://www.ihico.jp/var/ezwebin_site/storage/original/application/149ee9de3149aba2e1215fd5f9cd46ec.pdf).
- 902 Kaluza, P., Kolzsch, A., Gastner, M. T., & Blasius, B. (2010). The complex network of global
903 cargo ship movements. *Journal of the Royal Society*, *7*, 1093–1103.
- 904 Kritzinger, K. (2015). Personal Communication. 23 February, Stellenbosch.
- 905 Krug, M. J., & Tournadre, J. (2012). Satellite observations of an annual cycle in the Agulhas
906 Current. *Geophysical Research Letters*, *39*, L15607.
- 907 Lutjeharms, J. (2006). *The Agulhas Current*. Berlin: Springer.
- 908 Lutjeharms, J. R. E., & Roberts, H. R. (1988). The natal pulse: An extreme transient on the
909 Agulhas Current. *Journal Geophysical Research*, *93*, 631–645.
- 910 Marine Protection Services and Governance. (2014). *Unlocking the economic potential of South*
911 *Africa's Oceans*. Durban: Operation Phakisa.
- 912 Meehl, G. A., Goddard, L., Murphy, J., Stouffer, R. J., Boer, G., Danabasoglu, G. et al.
913 (2009) Decadal prediction. *Bulletin of the American Meteorological Society*, *90*, 14671485.
- 914 Meyer, I., & Van Niekerk, J. L. (2016). International Journal of Marine Energy Towards a practical
915 resource assessment of the extractable energy in the Agulhas ocean current. *International*
916 *Journal of Marine Energy*, *16*, 116–132. doi:10.1016/j.ijome.2016.05.010.
- 917 Meyer, I., Reinecke, J., Roberts, M., & van Niekerk, J. L. (2013). *Assessment of the ocean energy*
918 *resources off the South African coast*. Stellenbosch: Centre for Renewable and Sustainable
919 Energy Studies, Stellenbosch University.
- 920 Meyer, I., Reinecke, J., & Van Niekerk, J. L. (2014). Resource assessment of the Agulhas Current
921 for the purpose of marine energy extraction. In *5th International conference on ocean energy*.
922 Halifax.
- 923 Minesto. (2011). *DG-12 Technical Specifications*. Sweden: Minesto.
- 924 Minesto. (2015). Minesto—Power from Tidal and Ocean Currents, (n.d.). Retrieved November 23,
925 2015 from <http://minesto.com/>.
- 926 Mofor, L., Goldsmith, J., & Jones, F. (2014). *Ocean energy: technology readiness, patents,*
927 *development status and outlook*. Bonn: International Renewable Energy Agency [Online].
928 [http://www.irena.org/DocumentDownloads/Publications/IRENA_Ocean_Energy_report_2014.
929 pdf](http://www.irena.org/DocumentDownloads/Publications/IRENA_Ocean_Energy_report_2014.pdf). [2015, February 10].

- 930 Norton, M., Mansoldo, A., & Rivera, A. (2011). *Offshore grid study: analysis of the appropriate*
 931 *architecture of an irish offshore network*. Dublin: EirGrid Plc [Online]. http://www.eirgrid.com/media/2257_Offshore_Grid_Study_FA.pdf. [2015, June 20].
- 932 Renewable Energy Caribbean, (2014). Ocean Current Energy, an Untapped Resource. <https://renewableenergycaribbean.com/2014/09/01/the-potential-of-ocean-current-energy/>.
- 933 reNews, (2014). Minesto heading for Florida. <http://renews.biz/68909/minesto-heading-for-florida/>.
- 934 Rio, M.-H., Mulet, S., & Picot, N. (2014). Beyond GOCE for the ocean circulation estimate:
 935 Synergetic use of altimetry, gravimetry, and in situ data provides new insight into geostrophic
 936 and Ekman currents. *Geophysical Research Letters*, 41. doi:10.1002/2014GL061773.
- 937 Robinson, I. S. (2004). *Measuring the oceans from space*. Berlin: Springer.
- 938 Rouault, M. J., & Penven, P. (2011). New perspectives on the natal pulse from satellite
 939 observations. *Journal of Geophysical Research*, 116, C07013.
- 940 Rouault, M. J., Mouche, A., Collard, F., Johannessen, J. A., & Chapron, B. (2010). Mapping the
 941 Agulhas Current from space: An assessment of ASAR surface current velocities. *Journal of*
 942 *Geophysical Research*, 115, C10026.
- 943 Scott, R. B., & Wang, F. (2005). Direct evidence of an oceanic inverse kinetic energy cascade
 944 from satellite altimetry. *Journal of Physical Oceanography*, 35, 1650–1666.
- 945 Sink, K. Sink, K. J., Attwood, C. G., Lombard, A. T., Grantham, H., Leslie, R. et al. (2011).
 946 *Spatial planning to identify focus areas for offshore biodiversity protection in South Africa:*
 947 *Final report for the offshore marine protected area project*. Cape Town: South African
 948 National Biodiversity Institute.
- 949 U.S. Department of the Interior Minerals Management Service. (2007). *Programmatic environ-*
 950 *mental impact statement for alternative energy development and production and alternate use*
 951 *of facilities on the outer continental shelf: Final environmental impact statement*. USA: Bureau
 952 of Ocean Energy Management.
- 953 Van Zwieten, J. H. et al. (2014). Evaluation of HYCOM as a tool for ocean current energy
 954 assessment.
- 955 Van zwieten, J. H. et al. (2015). SS marine renewable Energy—Ocean current turbine mooring. In
 956 *Offshore technology conference*. Houston.
- 957 Wold, S., Esbensen, K., & Geladi, P. (1987). Principal component analysis. *Chemometrics and*
 958 *Intelligent Laboratory Systems*, 2, 37–52.
- 959
 960

Author Query Form

Book ID : 331464_1_En

Chapter No : 8



Springer

the language of science

Please ensure you fill out your response to the queries raised below and return this form along with your corrections.

Dear Author,

During the process of typesetting your chapter, the following queries have arisen. Please check your typeset proof carefully against the queries listed below and mark the necessary changes either directly on the proof/online grid or in the 'Author's response' area provided below

Query Refs.	Details Required	Author's Response
AQ1	References Beal et al. (2015) and Hass et al. (2013) are cited in the text but not provided in the reference list. Please provide the respective references in the list or delete these citations.	
AQ2	Please check whether the clarity of the sentence 'Desktop analysis by...30 to 45%' is OK.	

MARKED PROOF

Please correct and return this set

Please use the proof correction marks shown below for all alterations and corrections. If you wish to return your proof by fax you should ensure that all amendments are written clearly in dark ink and are made well within the page margins.

<i>Instruction to printer</i>	<i>Textual mark</i>	<i>Marginal mark</i>
Leave unchanged	... under matter to remain	Ⓟ
Insert in text the matter indicated in the margin	∧	New matter followed by ∧ or ∧ [Ⓢ]
Delete	/ through single character, rule or underline or ┌───┐ through all characters to be deleted	Ⓞ or Ⓞ [Ⓢ]
Substitute character or substitute part of one or more word(s)	/ through letter or ┌───┐ through characters	new character / or new characters /
Change to italics	— under matter to be changed	↙
Change to capitals	≡ under matter to be changed	≡
Change to small capitals	≡ under matter to be changed	≡
Change to bold type	~ under matter to be changed	~
Change to bold italic	≈ under matter to be changed	≈
Change to lower case	Encircle matter to be changed	≡
Change italic to upright type	(As above)	⊕
Change bold to non-bold type	(As above)	⊖
Insert 'superior' character	/ through character or ∧ where required	Υ or Υ under character e.g. Υ or Υ
Insert 'inferior' character	(As above)	∧ over character e.g. ∧
Insert full stop	(As above)	⊙
Insert comma	(As above)	,
Insert single quotation marks	(As above)	ƶ or Ʒ and/or ƶ or Ʒ
Insert double quotation marks	(As above)	ƶ or Ʒ and/or ƶ or Ʒ
Insert hyphen	(As above)	⊥
Start new paragraph	┌	┌
No new paragraph	┐	┐
Transpose	└┐	└┐
Close up	linking ○ characters	Ⓞ
Insert or substitute space between characters or words	/ through character or ∧ where required	Υ
Reduce space between characters or words		↑